

Optical and X-ray Studies of Ten X-ray Selected Cataclysmic Binaries¹

John R. Thorstensen

Department of Physics and Astronomy, Dartmouth College, Hanover NH, 03755, USA

Jules Halpern

Columbia Astrophysics Laboratory, Columbia University, 550 West 120th Street, New York, NY 10027, USA

ABSTRACT

We report on ground-based optical observations of ten cataclysmic binaries that were discovered through their X-ray emission. Time-resolved radial velocity spectroscopy yields unambiguous orbital periods for eight objects and ambiguous results for the remaining two. The orbital periods range from 87 min to 9.38 hr. We also obtained time-series optical photometry for six targets, four of which have coherent pulsations. These periods are 1218 s for 1RXS J045707.4+452751, 628 s for AX J1740.2–2903, 477 s for AX J1853.3–0128, and 935 s for IGR J19267+1325. A total of seven of the sources have coherent oscillations in X-rays or optical, indicating that they are intermediate polars (DQ Herculis stars). Time-resolved spectroscopy of one object, Swift J2218.4+1925, shows that it is an AM Herculis star, or polar, and IGR J19552+0044 may also be in that class. For another object, Swift J0746.2–1611, we find an orbital period of 9.384 hr and detect the spectrum of the secondary star. The secondary’s spectral contribution implies a distance of 900 (+190, –150) pc, where the error bars are estimated using a Monte Carlo technique to account for correlated uncertainties.

Subject headings: cataclysmic variables — X-rays: binaries — stars: individual (1RXS J045707.4+452751, Swift J0732.5–1331, Swift J0746.2–1611, AX J1740.2–2903, IGR J18173–2509, IGR J18308–1232, AX J1853.3–0128, IGR J19267+1325, IGR J19552+0044, Swift J2218.4+1925)

1. Introduction

Cataclysmic variables (CVs) are accreting binaries in which a late-type, usually dwarf star, donates mass via Roche-lobe overflow to a white dwarf (WD). In X-ray surveys, the occurrence

¹Based on observations obtained at the MDM Observatory, operated by Dartmouth College, Columbia University, Ohio State University, Ohio University, and the University of Michigan.

of different classes of CVs is correlated with the magnetic properties of the WD. At hard X-ray energies (> 10 keV), the population of CVs is dominated by magnetic systems, principally intermediate polars (IPs, or DQ Herculis stars), but also polars (AM Herculis stars). In polars, the magnetic field is strong enough to channel matter directly from the companion, along a narrow stream, onto the magnetic pole(s) of the WD. In the IPs, the magnetic field is not strong enough to prevent the formation of an accretion disk, but the disk terminates at a magnetospheric boundary; here again, matter is channeled onto the magnetic pole(s) of the WD. An IP is distinguished by its WD spin period, evident as a coherent oscillation in X-ray or optical emission from the rotating hot spot, at a shorter period than the orbital period of the binary. Sometimes the beat period between the spin and orbit periods is seen, due to reprocessed emission. In polars, the WD rotates synchronously with the binary orbit, or nearly so in the case of the few asynchronous polars (APs). Polars are also characterized by strong optical polarization, unlike the IPs.

X-ray spectra of CVs are correlated with their magnetic properties. The hard X-ray properties of magnetic CVs were reviewed recently by Scaringi et al. (2010). Their thermal bremsstrahlung X-ray emission presumably originates from the gravitational energy radiated in the shocked accretion column just above the surface of the WD, which accounts for the dominance of this class in hard X-ray (> 15 keV) surveys, such as those conducted by the *Swift* Burst Alert Telescope (BAT) and *INTEGRAL* IBIS. The *Swift*/BAT 70-month hard X-ray survey (Baumgartner et al. 2012) lists 55 CVs, of which 41 are magnetic: 31 IPs and 10 polars. Of the 33 CVs in the the fourth IBIS/ISGRI catalog (Bird et al. 2010), 25 are IPs and four are polars. The IPs outnumber the polars in hard X-ray surveys, presumably because of their higher accretion rates, and also because in polars the accretion may be more “blobby,” depositing some fraction of the energy directly onto the surface of the WD. The later hypothesis is motivated by observed blackbody radiation from polars with temperatures of tens of eV. Thus, the polars sometimes have two-component, soft and hard spectra, which explains why many were discovered in the soft X-ray survey of the *ROSAT* satellite.

Here we report on ground-based optical studies of ten CVs discovered by either *ASCA*, *Swift*/BAT, or *INTEGRAL* IBIS. As one might expect from the discussion above, nearly all these show evidence of being magnetic, such as relatively strong He II $\lambda 4686$ emission caused by X-ray photoionization, or coherent oscillations. Section 2 gives details of the observations and their analysis, and Section 3 describes the results for the individual objects. The objects observed are listed in Table 1, along with accurate celestial coordinates, approximate magnitudes, and spin periods where observed. Figure 1 gives finding charts of the objects for which we have our own direct images. Table 2 lists individual radial velocities, and Table 3 gives parameters of the best-fit sinusoids. Figures 2 and 3 show mean spectra, radial velocity periodograms, and folded radial velocities for all but two of the objects. We also present discovery data from the *Swift* X-ray Telescope (XRT) and Ultraviolet/Optical Telescope (UVOT), as well as time-series photometry and period analysis of detected pulsations in optical and X-ray. Our conclusions are summarized in Section 4.

2. Equipment and Techniques

All our optical data are from the MDM Observatory, which comprises the 1.3m McGraw Hill telescope and the 2.4m Hiltner telescope, on Kitt Peak, Arizona. High cadence photometry was carried out on six targets to search for spin periods that would originate from an IP. Five of these stars were observed with the the 1.3m, and a sixth with the 2.4 m. All ten of our radial velocity studies to search for the orbital periods used the 2.4m.

2.1. Time Series Photometry

For the time-series photometry in 2008–2012, we used the thinned, back-illuminated SITe CCD “Templeton,” a 1024×1024 chip with $24 \mu\text{m}$ pixels. In order to minimize readout time, the CCD was windowed and binned 2×2 to cover $4'.3 \times 4'.3$ with $1''.0$ pixels. Exposure times ranged from 10–30 s with a dead-time between exposures of only 3.6 s. For relatively blue stars we used a Schott BG38 filter to maximize throughput, while a reddened star required an R filter for optimal signal. Standard reductions used bias frames and sky flats, and aperture photometry was performed with the IRAF² routine `phot` and a single comparison star that was 2–3 magnitudes brighter than the variable. Landolt (1992) standard stars were used to calibrate the R -band frames. For the BG38 filter, an approximate magnitude was derived by averaging the B and R magnitudes of the comparison star in the USNO-B1.0 catalog (Monet et al. 2003).

Starting in 2013 we obtained time-series photometry with the 1.3-m telescope and an Ikon DU-937N CCD camera built by Andor Technology PLC. This integrated unit employs a thinned, backside-illuminated frame-transfer CCD with $13 \mu\text{m}$ square pixels and a 512×512 active area that subtends $140''$ at the 1.3-m. With 4×4 binning, the pixel scale was $1''.1 \text{ pixel}^{-1}$. Individual exposures were 10–30 seconds. We used Schott glass GG420 or BG38 filters, or a V -band filter. The dead time between exposures was only 11.92 milliseconds. The sensor was thermoelectrically cooled to -50 C for all observations. The Andor *Solis* software recorded each observation sequence as a data cube, giving only a start time and an inter-frame interval rather than a separate start time for each image; extensive tests showed that the nominal inter-frame interval was sufficiently accurate for our purposes. To reduce the data cubes, we subtracted median bias images and median dark images (scaled by exposure times), and divided by normalized median images of the twilight sky in the appropriate filter. We again measured magnitudes using `phot`, and referred these to a comparison star in the field. For the GG420 filter, this was the R magnitude of the comparison star in the USNO-B1.0.

The comparison star light curves often showed variations due to clouds, but these were for the most part thin enough that the differential photometry was usable. Sequences on individual

²IRAF is distributed by the National Optical Astronomy Observatory, which is operated by the Association of Universities for Research in Astronomy (AURA) under cooperative agreement with the National Science Foundation.

stars ranged from 2.4–6.5 hours. Period searches used a standard power spectrum analysis on these evenly sampled light curves. In two cases a slow trend was fitted out before calculating the power spectrum of the “detrended” light curve.

2.2. Spectroscopy

Nearly all of our radial velocity studies on the 2.4m used the modular spectrograph. The detector was one of two thinned SiTe CCDs, either “Echelle”, a 2048×2048 chip that covered 4300–7500 Å at 2.0 Å pixel^{-1} , or “Templeton”, the aforementioned 1024×1024 chip that covered 4660–6740 Å with the same dispersion. Wavelength calibrations were from Hg, Ne, and Xe comparison lamps taken during twilight, and we used the night-sky $\lambda 5577$ feature to track spectrograph flexure during the night. When it was clear, we observed flux standards during evening and morning twilight to calibrate the instrument response, but photometric conditions did not always prevail for our program-star observations, and seeing variations caused an unknown fraction of the light to be lost on the jaws of the $1''$ (projected) slit. Experience suggests that the fluxes in our average spectra are typically accurate to $\sim 20\%$. In addition, our modular spectrograph setup sometimes produces unrealistic continua, which fortunately tend to average out over many exposures. Our slit was oriented north-south by default – parallel to atmospheric dispersion on the meridian. At large hour angles and zenith distances, we rotated the instrument to orient the slit close to the parallactic angle³. This was often needed, because we were trying to find orbital periods; observations far from the meridian are required in order to suppress ambiguities in the daily cycle count. (For one target, Swift J0732.5–1331, we could not optimize the slit position angle because we needed to avoid a nearby brighter star.)

Our 2012 December velocities of IGR J19552+0044 are from the modular spectrograph mounted on the 1.3m telescope. The setup and procedures were identical to those used at the 2.4m, except that we did not rotate the instrument to the parallactic angle. The 1.3m and 2.4m telescopes are both $f7.5$, so the image scale of the 1.3m is proportionally smaller than that of the 2.4m. Because the same physical slit size was used on both telescopes, the projected slit width was larger at the 1.3m. Consequently, alignment with the parallactic angle is less critical than with the larger telescope.

We reduced our spectra using standard IRAF and Pyraf routines for bias subtraction, flat-fielding, wavelength calibration, and flux calibration. To extract one-dimensional spectra, we used an implementation of the algorithm published by Horne (1986). We measured emission-line radial velocities using convolution algorithms described by Schneider & Young (1980) and Shafter (1983). When a cool star was detectable in the spectrum, we used the Kurtz & Mink (1998) implementation

³The most recent version of the *JSkyCalc* program, available at JRT’s website, includes a parallactic angle optimization tool. Note that the dispersion grows as $\tan z$, rather than $\sec z$, so there is no large “flat spot” around the zenith as there is with extinction.

of the Tonry & Davis (1979) cross-correlation to measure its velocity; for the template, we used a velocity-compensated sum of 76 observations of late G and early K-type IAU velocity standards. To measure synthetic magnitudes from our spectra we used the Bessell (1990) tabulation of the V passband and the IRAF *sbands* task.

The main purpose of our spectroscopy was to determine the periodicity in the radial velocities (which is identical to the orbital period P_{orb} in nearly all cases). We searched for periods in the time series using a “residual-gram” algorithm (Thorstensen et al. 1996). The observability constraints imposed on observations from a single site inevitably lead to some ambiguity in the daily cycle count; when these appeared significant, we used the Monte Carlo method of Thorstensen & Freed (1985) to assess the robustness of our choice of orbital period. We use the “discriminatory power” statistic from that test, which is the fraction of Monte Carlo trials that result in the correct period being chosen, and not an alias, by virtue of having the smallest residuals.

3. Individual Objects

Targets for this study were selected via a variety of methods that were likely to yield magnetic CVs. These include followup *XMM-Newton* observations showing periodicities from *ASCA* sources in the Galactic plane, *Swift* BAT sources for which pointed observations with the XRT found rapidly varying X-rays and a relatively bright or blue optical counterpart, and *INTEGRAL* IBIS sources already identified spectroscopically as CVs. In this section, we detail our observations and results on the individual objects.

3.1. 1RXS J045707.4+452751

The IR counterpart of this *ROSAT* X-ray source was identified by Kaplan et al. (2006) from a *Chandra* image, but not classified. It was detected in the *Swift* BAT survey (Voss & Ajello 2010; Cusumano et al. 2010a), and by *INTEGRAL* IBIS (Krivonos et al. 2010), then classified as a CV when Masetti et al. (2010) obtained a spectrum of the optical counterpart. Masetti et al. (2010) give coordinates and a finding chart for the wrong star; Fig. 1 and Table 1 give the correct identification. Our spectrum (Fig. 2) appears nearly identical to theirs, but with a slightly lower continuum level and better signal-to-noise ratio. In agreement with Masetti et al. (2010) we see He II $\lambda 4686$ at less than half the strength of $H\beta$; our signal-to-noise reveals He II $\lambda 5411$ as well, with an emission equivalent width (EW) of $\approx 1.7 \text{ \AA}$. We detect the diffuse interstellar bands (DIBs) at $\lambda 5780$ (0.7 \AA EW) and $\lambda 6283$ (1.0 \AA EW). Yuan & Liu (2012), in a review of SDSS spectra, find on average that $EW(5780) = 0.61 \times E_{BV}$ and $EW(6283) = 1.26 \times E_{BV}$, with considerable scatter, so these band strengths are roughly consistent with $E(B - V) \approx 1.0$. The Schlegel, Finkbeiner, & Davis (1998) extinction map gives $E(B - V) = 1.05$ at this location (or 0.90 if one adopts the 14% correction recommended by Schlafly & Finkbeiner 2011), in excellent agreement with the DIB estimate. Our

spectrum implies $V = 17.5$; taking $A_V/E(B - V) = 3.1$ gives an extinction-corrected $V = 14.7$. The object lies at Galactic coordinates $l = 160.^\circ 97$, $b = +1.^\circ 52$, so the sizeable reddening is not unexpected.

The object appears to be a novalike variable of some kind. At a distance of 1 kpc, it would have $M_V \sim +4$, comparable to other novalike variables (Warner 1995). Masetti et al. (2010) estimate $A_V \sim 0$ and $d \sim 500$ pc for this object (their Table 2); the substantial reddening we find, and the similarity to a novalike variable, suggest that they underestimate both these quantities.

Our $H\alpha$ emission velocities (Fig. 2) did not yield an unambiguous orbital period, but we do detect a significant periodicity consistent with either $P_{\text{spec}} \approx 0.258$ d (3.87 cycle d^{-1}) or ≈ 0.200 d (4.98 cycle d^{-1}). These are daily cycle count aliases. We also do not know how many cycles elapsed between our observing runs. We are at least confident that the orbital period is longward of the 2–3 hr “gap” in the CV period distribution.

Figure 4 shows a 6.8-hour photometric sequence we obtained with the Andor camera on 2013 January 4, using a GG420 filter. The magnitude scale is calibrated to the R magnitude of the comparison star from the USNO-B1.0 catalog. The main period detected is 1208 ± 12 s, which is likely to be the rotation period of a magnetized white dwarf (or possibly half the period). Detrending the data with a 0.258-d period improves the power spectrum slightly. The night was mostly clear, though the comparison star showed evidence of occasional light clouds. The 1208-s period was not detected on two subsequent nights, but our observations were shorter then, and we used a BG38 filter, which proved to be less sensitive than the GG420.

We obtained additional time series with the same setup on 2013 March 1–3 (Fig. 5). These displayed the periodic signal very clearly, and a coherent fit to the three consecutive nights yields $P = 1218.7 \pm 0.5$ s, which we adopt as the most precise value. There is no evidence from the folded light curves that the true period is twice this value. Masetti et al. (2010) suggested that the system is not magnetic, on the basis of its relatively weak He II emission, but the detection of a coherent modulation shows that it actually is magnetic. We have examined the existing *Chandra* and *Swift* XRT data on 1RXS J045707.4+452751, but they are too sparse to reveal the period.

3.2. *Swift* J0732.5–1331= V667 Puppis

A flurry of discovery surrounded this source in early 2006. First, Ajello et al. (2006) detected it using the *Swift* Burst Alert Telescope (BAT) and suggested it was identical to a *ROSAT* source coincident with a $B \sim 15$ mag star. Masetti et al. (2006) found emission lines, confirming the identification; Patterson et al. (2006) found a periodic modulation at 512.42(3) s, and pulsations at the same frequency were soon found by Wheatley et al. (2006) using the *Swift* XRT, confirming the IP nature of the source. Further confirmation of the spin period was found by Butters et al. (2007) in *RXTE* data. Patterson et al. (2006) also obtained a spectrum showing a strong G-type stellar contribution to the spectrum, but were unable to detect the ellipsoidal modulation that would be

expected if the G-star were the secondary. The puzzle of the missing ellipsoidal modulation was resolved when Marsh et al. (2006) found the purported counterpart to be a close optical pair, with the fainter of the two stars being the bluer, pulsating object. Torres et al. (2006) found significant emission line velocity variations, but were unable to determine a period. We then obtained more extensive velocities and found the 0.2335-d period reported briefly in Thorstensen et al. (2006). We present these observations in greater detail here.

The spectrum (Fig. 2) shows relatively weak emission, with He II $\lambda 4686$ around the same strength as H β . There is a broad bump in the continuum between 5000 Å, and 6200 Å, but we cannot be sure this is real; the strong upsweep into the blue also appears unphysical. Because of the crowding star, we were unable to follow our usual practice of keeping the slit near the parallactic angle; instead, we used slit position angles between -36° and -44° . Close examination of the spectrum reveals weak, stationary absorption features around $\lambda 5175$, which we believe are from the crowding star; the crowding star may also be responsible for the continuum bump.

The H α emission line velocities show a very clear modulation at 5.61 hr. Figure 6 shows a grayscale phase-averaged spectrum synthesized from our spectra. To prepare this, we (1) rectified our spectra to the continuum, (2) hand-edited the individual spectra to remove radiation events and other artifacts, (3) constructed each line of the image from a weighted average of spectra close to the phase represented by that line⁴, and (4) stacked the lines to form the two-dimensional image. There is a rather faint double-peaked profile, with a modest velocity amplitude, and a stronger component that undergoes an “S-wave” modulation between the velocities of the peaks. This may arise in a hot spot, where the mass-transfer stream strikes the accretion disk. On the other hand, the sizeable radial velocity amplitude is reminiscent of an AM Her star (or polar), in which there is no accretion disk and therefore no hot spot. In polars, the accretion column produces large infall velocities, and hence strong velocity modulation, but the line profile does not support this interpretation. AM Her stars tend to show broad, asymmetric line wings, which move with the orbit (as in Swift J2218, Section 3.10). These are not seen here, so this appears not to be a polar.

We obtained three sets of *UBVI* images on 2006 March 13 UT, with the 2.4m telescope. Conditions were photometric, and the seeing was $\approx 1''$, which was good enough to resolve the X-ray source from the nearby star, as shown in an *I*-band image in Figure 1. To measure magnitudes, we used the IRAF implementation of DAOPHOT, which fits point spread functions. The position in Table 1 is from this fit. For V667 Pup, we found $V = 15.8$, $B - V = +0.3$, $U - B = -0.7$, and $V - I = +0.6$, with fluctuations between measurements of ~ 0.05 mag. The companion averaged $V = 14.29$, $B - V = +0.66$, $U - B = +0.13$, and $V - I = +0.75$, with somewhat smaller fluctuations.

⁴The weighting function used was a Gaussian in phase, with a full-width at half-maximum of ~ 0.05 cycles, truncated ± 0.05 cycles from the central phase.

3.3. Swift J0746.2–1611

This is an unclassified source in the *Swift* BAT survey (Voss & Ajello 2010; Cusumano et al. 2010a), where it was associated with the *ROSAT* source 1RXS J074616.8–161127. It was also detected by the *BeppoSAX* Wide Field Camera (Capitano et al. 2011). We identified it with a highly variable X-ray source in several *Swift* XRT observations (Fig. 7), as well as with a UV-bright counterpart in the *Swift* UVOT (Fig. 8). The *Swift* observations are too sparse to reveal any periods. We are not aware of any prior optical work on Swift J0746.2–1611.

Its spectrum (Fig. 2), includes a significant contribution from a late-type secondary star as well as the typical emission lines. The secondary’s velocities give period near 9 hr, which we refined over several observing runs to 0.39101(1) d. The emission-line velocities are much less steady, but corroborate the absorption-line period (and eliminate the possibility that the absorption lines are from a distant companion to the binary, or chance superposition).

By scaling and subtracting spectra of stars classified by Keenan & McNeil (1989), and searching for good cancellation of the secondary’s features, we determined the secondary’s spectral type to be $K4 \pm 2$ subclasses, and quantified its contribution to the spectrum. We then computed a distance based on the following procedure, which is described in more detail by Thorstensen et al. (2012) and Peters & Thorstensen (2005). (1) The Roche-lobe constraints and P_{orb} determine the physical size of the secondary (with a weak dependence on the secondary’s assumed mass). (2) The secondary’s spectral type determines its surface brightness. (3) The spectral decomposition gives an apparent magnitude for the secondary’s contribution. (4) We correct for reddening, and determine the distance.

All of these steps involve uncertainties; a crude estimate of the uncertainty in the final distance can be had by propagating the errors in the standard manner, and that is the procedure we have followed in the past. This is not entirely satisfactory, because some of the parameters can be correlated. Most importantly, metal lines are stronger at later spectral types, so normalization of the secondary star’s spectral contribution – which is estimated by looking for the best subtraction of the line features – tends to be correlated with the spectral type. We therefore implemented a Monte Carlo procedure, as follows. First, for each assumed secondary spectral type, we defined a permitted range of secondary-star V magnitudes, based on our decompositions. We also assumed a normally-distributed 0.2 mag uncertainty in our spectrophotometric normalization. In this case, acceptable decompositions could be found for K2 through K6; we assigned discrete probabilities of 0.3 to K4, 0.2 to K3 and K5, and 0.15 to K2 and K6. For the surface brightness at each spectral type, we used an analytical fit to surface brightness vs. spectral type data presented by Beuermann et al. (1999), and assumed a ± 0.2 mag range of uncertainty in this calibration. For the secondary star mass we took $M_2 = 0.65 \pm 0.2$, based on the Baraffe & Kolb (2000) evolutionary calculation; we took masses to be uniformly distributed within this range and used the random masses to compute the secondary’s radius. The surface brightness and radius then gave the absolute magnitude, which combined with the secondary’s V gave an apparent distance modulus.

For reddening, we used the Schlegel, Finkbeiner, & Davis (1998) maps to establish an upper limit of $E(B - V) = 0.18$, and – since the star is within the dust layer and evidently not exceptionally distant – we took the reddening to be $E(B - V) = 0.10 \pm 0.05$, with an upper cutoff at 0.18 and a lower cutoff at 0.02⁵. With all these ingredients in place, we computed 10,000 distances, drawing each ingredient from its assumed distribution every time. The resulting distances are shown in Figure 9; the median and the ends of the 68% confidence error bars give a distance of 900 (+190, –150) pc.

We searched for optical pulsations in this source using the Andor camera on three consecutive nights in 2013 January. The source varied erratically by several tenths of a magnitude, but we were unable to detect any periodicity. The longest of the nightly light curves is shown in Figure 10. Swift J0746.2–1611 is a novalike variable, but whether it is also a DQ Her star remains an open question.

3.4. AX J1740.2–2903

Sakano et al. (2000) detected this hard source in an *ASCA* observation (in which they also detected another pulsating source, AX J1740.1–2847). AX J1740.2–2903 was also detected by *INTEGRAL* IBIS (Bird et al. 2010). Farrell et al. (2010) detected a 626-s pulse in *XMM-Newton* data, and around the same time Malizia et al. (2010) improved the position, also with *XMM-Newton* data, but they gave a position that was incorrect by 25". We had independently analyzed the same *XMM-Newton* data, finding the optical counterpart (Halpern & Gotthelf 2010a) and the pulsations, both in X-ray and then in optical (Halpern & Gotthelf 2010b). Masetti et al. (2012) present a optical spectrum, which appears similar to ours.

We obtained time-series photometry on one night each in 2010 June and 2012 June (Fig. 11). Because of moderate extinction to the source, only the *R* band gave sufficient signal. A period was clearly detected in power spectra of the light curves, with values of 622.7 ± 4.5 s and 628.6 ± 2.3 s, respectively, in 2010 and 2012. These agree with the X-ray period of 626 ± 2 s measured by Farrell et al. (2010), or 623 ± 2 s in our own analysis of the same X-ray data. The pulsed amplitude in the optical was ≈ 0.16 mag peak-to-trough in 2010, and ≈ 0.11 mag in 2012. The shape of the single-peaked light curve is similar to that of the X-ray, except that the latter is much more highly modulated (Fig. 12).

The spectrum (Fig. 2) shows prominent $H\alpha$, with 45 Å emission EW, and flux $\sim 5 \times 10^{-15}$ erg cm⁻² s⁻¹. The line is single-peaked and somewhat narrow for a CV, with FWHM ≈ 680 km s⁻¹. The continuum slopes upward toward the red, suggesting substantial reddening, and the synthesized $V = 19.1$ is on the faint side. The X-ray spectral fits of Farrell et al. (2010) require a column density

⁵The reddening was small enough and uncertain enough that we ignored the 14% correction recommended by Schlafly & Finkbeiner (2011).

$N_{\text{H}} \approx 4 \times 10^{21} \text{ cm}^{-2}$, which would be equivalent to $A_V \approx 2$ if it is all intervening. An absorption feature with $\text{EW} \approx 2.2 \text{ \AA}$ is present at 6283 \AA , and there is a hint of a feature ($\text{EW} \approx 0.6 \text{ \AA}$) near 5780 \AA ; these are probably the DIBs. In our reduction we correct approximately for telluric features, but because of the inevitably large airmass at this southerly declination it is likely that the $\lambda 6283$ DIB is blended with a telluric feature that strongly overlaps it (Jenniskens & Desert 1994 show both the DIB and the telluric feature in detail).

Our emission-line velocities give a best period near 0.237 d , or 5.7 hr (Table 3), but 0.314 d (7.52 hr), which is 1 cycle d^{-1} lower in frequency, cannot be entirely ruled out. A Monte Carlo test gives a discriminatory power (Thorstensen & Freed 1985) of around 0.98 for our time series, so the period determination is reasonably secure. The results presented here, especially the short orbital period, rule out the hypothesis of Farrell et al. (2010) that AX J1740.2–2903 is symbiotic binary.

3.5. IGR J18173–2509

Masetti et al. (2009) identified the counterpart using a Swift follow-up observation reported by Landi et al. (2008), and obtained a spectrum. Our spectrum (Fig. 3) closely resembles theirs, with strong $\text{H}\alpha$ emission and no obvious indication of reddening. Masetti et al. (2009) obtained direct images that gave $R = 17.2 \pm 0.1$. Our direct images gave $V = 16.9 \pm 0.2$, in rough agreement, and our spectra gave a synthesized $V = 17.1$.

A spin period of $1690 \pm 18 \text{ s}$ was measured by Bernardini et al. (2012) in the B filter of the *XMM-Newton* Optical Monitor, while the X-ray power in the same observation is confined to the first harmonic at $831.7 \pm 0.7 \text{ s}$. The latter is consistent with $830.70 \pm 0.02 \text{ s}$ measured in *Swift* XRT data (Nichelli et al. 2009). Bernardini et al. (2012) estimate $P_{\text{orb}} = 8.5 \pm 0.2 \text{ hr}$ from sidebands of the X-ray, and $P_{\text{orb}} = 6.6 \pm 0.3 \text{ hr}$ by folding the X-ray light curves and looking for a modulation.

The mean spectrum (Fig. 3) shows a blue continuum and strong emission lines. $\text{H}\alpha$ is double-peaked, with a weaker blue peak near -270 km s^{-1} and a stronger red peak near $+330 \text{ km s}^{-1}$. The line profile is steep-sided, with a $\text{FWHM} \approx 1160 \text{ km s}^{-1}$. A greyscale representation of the $\text{H}\alpha$ line (Fig. 6) shows that the asymmetry of the red and blue persists throughout the orbital cycle, and is not caused by uneven sampling of an S-wave. A very weak S-wave may be present, but it cannot be traced across the center of the line.

The radial velocities show a periodicity at 91.9 min , or $15.67 \text{ cycle d}^{-1}$. Because of the southerly declination and the time of year the data were taken, the velocities span only 5.7 hr of hour angle, so there is some uncertainty in the daily cycle count. Running the Monte Carlo test against either one of the flanking aliases gives a discriminatory power of 93% ; because there are two flanking aliases of nearly equal strength, the discriminatory power against the two is below 90% . The choice of radial-velocity period is therefore not entirely reliable.

The coherent $830/1660 \text{ s}$ modulation shows clearly that this is an IP. A relatively small number

of such systems have orbital periods short of the 2–3 hr “gap”. Ritter & Kolb (2003), in their on-line catalog⁶, list 50 objects as definite IPs; of these, only four (V1025 Cen, HT Cam, DW Cnc, and EX Hya) have orbital periods shorter than the 91.9 min period found here; also, another object in the present sample, AX J1853.3–0128 (Section 3.7) has an 87-minute period.

While the radial-velocity period is very likely to be the orbital period, it is possible that it is not. In V455 And (Araujo-Betancor et al. 2005), the emission-line radial velocities follow persistent, but incoherent, 3.5-hour period, while P_{orb} is only 81.08 min. The radial velocity of DW Cnc shows two periods, 86.1 and 38.6 min, which are probably the orbital period and the white-dwarf spin period respectively (Patterson et al. 2004; Rodríguez-Gil et al. 2004). While the much longer P_{orb} candidates proposed by Bernardini et al. (2012) are possible, neither of these is definitive, and we think the radial velocity period is more likely to be correct. This object could use further spectroscopy to untangle remaining cycle-count uncertainties and determine whether our period is coherent over intervals longer than our week-long observing run – if so, the case for the $P_{\text{orb}} = 91$ min would be significantly stronger.

3.6. IGR J18308–1232

The optical counterpart of this source was identified spectroscopically by Parisi et al. (2008), and Masetti et al. (2009) show the spectrum. We have some direct images; one set of *BVI* photometry images from 2010 June gives $V = 17.95$, $B - V = +0.34$, and $V - I = 1.171$. Masetti et al. (2009) quote $R = 17.0$, in rough agreement. Bernardini et al. (2012) found a spin period of 1820 ± 2 s in *XMM-Newton* data, and find a candidate $P_{\text{orb}} = 4.2$ h from a weak, presumed X-ray sideband. The X-ray spin period appears to be reliable, but the evidence for an orbital period is tentative.

The mean spectrum resembles the one published by Masetti et al. (2009); it shows $\text{H}\alpha$ with an emission EW of ~ 20 Å and a FWHM of ~ 700 km s⁻¹. The line profile is slightly double-peaked, with the peaks at ± 150 km s⁻¹ from the line center. The Na I D doublet is present in absorption, with a combined EW ~ 1.7 Å. The Na I D line widths are unresolved, and the velocity is constant, indicating that they are interstellar. In addition, the DIB at $\lambda 5780$ is present with EW ~ 0.5 Å, which implies $E(B - V) \sim 0.8$ based on the correlations found by Yuan & Liu (2012), or $A_V \sim 2.5$ assuming $A_V/E(B - V) = 3.1$. Masetti et al. (2009) estimate a much lower extinction, $A_V = 0.67$. If $E(B - V)$ really were as large as 0.8, our observed color would imply $(B - V)_0 \sim -0.4$, which is too blue for a novalike variable (see, e.g., the colors compiled by Bruch & Engel 1994), so the reddening is likely to be significantly less. As an illustration, adopting $E(B - V) = 0.4$, or $A_V \sim 1.3$, gives $V_0 = 16.7$. Novalike variables have absolute magnitudes broadly similar to dwarf novae in outburst – $M_V \sim +4$ (Warner 1995; see also Beuermann et al. 2004), which yields a distance around 3 kpc, much larger than the ~ 320 pc distance suggested by Masetti et al. (2009), who assumed $M_V \sim +9$.

⁶available at <http://www.mpa-garching.mpg.de/RKcat/>; we used Version 7.16

While at least one IP has an absolute magnitude this faint (EX Hya; Beuermann et al. 2003), we think IGR J18308–1232 is likely to be considerably more luminous. Later, we find $P_{\text{spec}} \sim 5.4$ h; at that period the semi-empirical donor sequence derived by Knigge (2006) predicts that the donor should have spectral type M0 and $M_V = +8.2$. We see no sign of a secondary contribution in our spectrum, which suggests $M_{V0} < 7$. Along this line of sight ($l = 19.^\circ 45, b = -1.^\circ 20$) the reddening map of Schlegel, Finkbeiner, & Davis (1998) gives a total Galactic extinction of $E(B - V) = 4.9$; clearly, this object is in front of most of the dust.

The H α radial velocities give a period near 5.4 hr. If the frequency is 1 cycle d $^{-1}$ higher, the period is 4.39 hr, close to the period derived by Bernardini et al. (2012). Our velocities span almost 6.5 hr of hour angle, and the Thorstensen & Freed (1985) Monte Carlo test gives a discriminatory power of over 95% for our alias choice. Nonetheless, we cannot entirely rule out a cycle-count error. We obtained data on four observing runs with a total span of 778 days, so the period determination suffers from multiple ambiguities in the longterm cycle count as well as a daily ambiguity. The period uncertainty in Table 3 is based on the lengths of the individual observing runs.

3.7. AX J1853.3–0128

The periodic nature of this source in a 20 ks *XMM-Newton* observation taken on 2004 October 25 was noted by Munro et al. (2008) and Hui et al. (2012). Both authors concluded that the period is 238 s, supporting an IP classification. However, detailed inspection of the pulsed X-ray light curve reveals that the true period is twice this value. Figure 12 shows the energy-dependent pulse profiles folded at our derived period of 476.0 ± 0.2 s. Even though most of the power falls at the first harmonic because the hard X-ray pulse is double peaked, it is apparent that the two minima of the light curve are of unequal heights, the difference growing more prominent toward low energies until the soft X-ray pulse ($E < 1$ keV) has a single broad plateau and barely two maxima. Folding at half the correct period was largely responsible for the small modulation at the lower energies in the pulse profiles displayed in Hui et al. (2012).

We are not aware of any prior optical work on AX J1853.3–0128. We identified its optical counterpart from the *XMM-Newton* position, and obtained time-series photometry on the 1.3m McGraw-Hill on 2007 June 19 through a BG38 filter. This 3-hr run, while displaying flickering typical of a CV, did not reveal a periodic signal. However, a repeat of this observation in a 6.5-hr run on 2012 June 20 (Fig. 11) clearly confirms the 476 s period and the IP classification. We find $P = 477.6 \pm 1.0$ s. Unlike the X-rays, the majority of the optical power (in the broad BG38 filter) is in the fundamental, although the first harmonic is also prominent. The binned light curve has an amplitude of only 0.07 mag peak-to-trough, but its pulse shape is strikingly similar to that of the soft X-rays, a broad, flat plateau with a slight dip in the middle. It is possible that the double-peaked X-ray light curve is indicating emission from both poles because the peaks are 180 $^\circ$ apart. However, in the optical light curve the peaks are not 180 $^\circ$ apart.

The emission lines in the mean spectrum (Fig. 3) are unusually strong and quite broad; $H\alpha$ has an EW of 230 Å and a FWHM ~ 1350 km s $^{-1}$. All the emission lines are slightly double-peaked; in $H\alpha$, the blue peak is at -360 km s $^{-1}$ and the red at $+200$ km s $^{-1}$. The red peak is slightly stronger than the blue peak. The $H\alpha$ radial velocities are modulated on an 87-minute period, with no ambiguity in daily cycle count. In the optical, AX J1853.3–0128 appears to be a near-twin of IGR J18173–2509 (Section 3.5).

3.8. IGR J19267+1325

Steeeghs et al. (2008) identified this as a cataclysmic binary using the IPHAS $H\alpha$ survey (Witham et al. 2007) and a Chandra localization (Tomsick et al. 2008, 2009). Masetti et al. (2009) show a spectrum. Evans et al. (2008) detected pulsations at 938.6(+5.6,–5.9) s in Swift-XRT data, showing that this is a DQ Her-type system. They also detected some evidence for a period at $\sim 16500(+1900, -1500)$ s, which they suggested might be an orbital period.

Our mean optical spectrum shows a red-sloping continuum with strong, single-peaked emission lines – $H\alpha$ has EW ~ 80 Å, and FWHM ~ 900 km s $^{-1}$. He II $\lambda 4686$ is about half the strength of $H\beta$, and He II $\lambda 5411$ is present as well.

Most of our optical spectra were obtained on adjacent nights in 2008 September, and the remainder on three nights in 2009 June. The data define an unambiguous 3.4-h orbital period (Table 3), but with an unknown cycle count in the 280-day gap between observations. Our period amounts to 12416 ± 35 s, so it appears that the 16500-s period detected by Evans et al. (2008), if persistent, is unrelated to the orbit.

We obtained time series photometry of IGR J19267+1325 in the R filter on four consecutive nights in 2008 August (Fig. 13). A spin period is detected on each night individually, and a coherent power spectrum of all four nights gives $P = 935.1 \pm 0.2$ s, in agreement with the X-ray period of Evans et al. (2008). On one night, August 21, the strongest peak was at 1009 s, which could possibly be the sideband, or beat between the spin and the orbit.

3.9. IGR J19552+0044

Masetti et al. (2010) give a finding chart and a spectrum showing unusually strong Balmer lines together with He I and some He II emission. Our spectra appear generally similar to theirs; the top panel of Fig. 14 shows the mean of our 2013 June spectra. HeII $\lambda 4686$ and $\lambda 5411$ appear strongly.

We have radial velocities from three observing runs late in 2012, one in 2013 February, and limited data from 2013 June. Unfortunately, we could not determine an unambiguous rough orbital period. The most extensive and ‘cleanest’ data are from two nights in 2012 October, which favored

a radial-velocity frequency near $17.17 \text{ cycle d}^{-1}$ (or 83.9 min), with aliases spaced by 0.5 cycle d^{-1} , reflecting a two-day gap between the two nights of observation. The 1-day baselines in the remainder of the data eliminate every other one of these aliases, but when all the data are analyzed together there is strong scatter in the velocity curve, evidently reflecting changes in the state of the source from run to run. Fig. 14 (middle panel) shows the periodogram of all our velocities; it is badly affected by a combination of large variations in the source and limited sampling in the various observing runs. We very tentatively adopt a frequency (marked by a question mark) that is consistent with the 2012 October data and which yields a folded velocity fit (lower panel of Fig. 14) that is roughly consistent with the remainder of the velocities. Although this is very crude, the velocities clearly indicate a period shortward of the 2-3 hour period gap.

We obtained brief photometric time series of IGR J19552+0044 in 2012 June (Fig. 11) which showed no evidence of a coherent pulsation, although the star flickered by over 1 magnitude on a time scale of minutes. On three nights in 2013 June we obtained more extensive differential photometry using the Andor camera and a V filter. To convert the 2013 June time series to approximate standard V magnitudes, we used the SDSS Data Release 9 to estimate $V = 16.94$ for the main comparison star, which lies 8 arcsec west and 39 arcsec north of IGR J19552+0044. The light curves (Fig. 15) show an approximately periodic brightening on a timescale similar to our adopted radial-velocity period. A sinusoidal fit to these data gives a best period near 0.0565 d ($\sim 81 \text{ min}$), or $17.7 \text{ cycle d}^{-1}$. Our best radial velocity period amounts to $17.23 \text{ cycle d}^{-1}$, so the photometric modulation does not appear to be coherent on the radial-velocity period; constraining the radial-velocity period to a range consistent with the apparent photometric period results in very poor fits.

The photometry from 2013 Jun 13 UT also shows flickering with a timescale of 5 to 10 minutes and an amplitude of up to ~ 2 magnitudes. This is not an artifact, as it is obvious from inspection of the original images. A power-spectrum analysis of that night’s data (Fig. 15, lower panel) showed no coherent signal consistent with the flickering time scale.

It is not obvious how to classify this object. The absence of any coherent pulse is consistent with an AM Her star, or polar. However, in our limited data we do not see strong, asymmetric line wings or sharp moving features in our spectra (as we see in Swift J2218.4+1925; see Section 3.10). Time-resolved polarimetry might clarify the classification.

3.10. Swift J2218.4+1925

This was detected as a hard X-ray source in the *Swift* BAT (Cusumano et al. 2010b; Baumgartner et al. 2012), and localized by the *Swift* XRT in observations on 2009 August 2 and 4. It is coincident with 1RXS J221832.8+192527. Its highly variable *Swift* X-ray light curves are shown in Figure 7. We present a finding chart from the *Swift* UVOT in Figure 8, which shows a UV-bright counterpart. We reported briefly on optical observations of Swift J2218.4+1925 in Thorstensen & Halpern

(2009), and give more details here. We are not aware of any other optical work on this source.

The average spectrum (Fig. 16) shows strong, broad emission lines, and He II $\lambda 4686$ is clearly detected. The amplitude of the H α radial velocity modulation is large, and the 129-min period is determined without ambiguity. The large velocity amplitude, and extensive line wings, suggest that this is a polar, or AM Herculis star, in which much of the emission comes largely from a synchronously-rotating, magnetically-channelled accretion column.

The lower panel of Fig. 16 shows a greyscale phase-averaged spectrum synthesized from our spectra, prepared using the procedure discussed in Section 3.2. The image reveals two distinct emission-line components: one of them is diffuse and has a large velocity amplitude, and the other is sharper, has a lower amplitude, and is visible over only part of the phase. The diffuse component very likely arises in an accretion column, and the sharp component is probably radiation reprocessed on the side of the secondary star that faces the white dwarf. The sharp component comes into view around its maximum positive velocity, and fades from view near its minimum velocity; this is just as expected from a heated face. The behavior of the emission-line profiles with phase closely resembles that of known polars (Schwope et al. 1999), so we conclude that Swift J2218.4+1925 is another example of this type.

Using the single-trail image, we estimated radial velocities of the sharp component by eye and fit them with a sinusoid, which had $T_0 = \text{HJD } 2455070.7050(7)$ and $K_2 = 282(15) \text{ km s}^{-1}$. The epoch T_0 falls 0.26 cycle later than the T_0 listed in Table 3; it corresponds to the blue-to-red transition of the sharp component, so it very likely represents the inferior conjunction of the secondary star. The epoch in Table 3 is based on “whole-line” measurements, which do not have a simple physical interpretation but which do define the period well.

If the masses of the component stars are broadly typical for CVs of this period, and the sharp component traces the motion of the secondary, then the orbital inclination i is unremarkable. For illustration, taking $M_1 = 0.75 M_\odot$ and $M_2 = 0.2 M_\odot$ (using Knigge 2006 as a guide), our K_2 implies $i = 50^\circ$, so eclipses are unlikely.

4. Conclusions

The selection of CVs studied here does not comprise a well-defined “sample” in any quantitative sense. However, selected on the basis of hard X-ray detection and variability, they lead to the expected result that at least eight of the ten are magnetic CVs, of which seven are of the IP class, which is the dominant CV population in hard X-ray surveys. Their spin and orbit periods are within the ranges previously observed for members of their classes. Here we summarize the most interesting conclusions about the individual objects, and offer recommendations for further work on some of these stars.

We obtained firm orbital periods for eight of the ten objects, ranging from 87 min to 9.38 hr.

Two of the IPs studied here are somewhat unusual in having short orbital periods, IGR J18173–2509 (91.9 min) and AX J1853.3–0128 (87 min). IGR J18173–2509 has the unusually large value of $P_{\text{spin}}/P_{\text{orb}} = 0.3$, and is an exception to the observation of Scaringi et al. (2010) that all hard X-ray-detected IPs have $P_{\text{spin}}/P_{\text{orb}} < 0.1$. The spin period of AX J1853.3–0128, 476 s, is twice the value previously published on the basis of X-ray data. A careful analysis reveals its fundamental period in X-rays as well as in optical.

We obtained the first evidence for the magnetic nature of 1RXS J045707.4+452751 by detecting a persistent 1218 s period, and confirmed the IP nature of IGR J19267+1325 by detecting its 935 s period in the optical over four nights.

The previously debated nature of AX J1740.2–2903 is resolved in favor of an IP by showing that its 626 s X-ray (spin) period is also present in the optical, and by discovering its 5.7 hr orbital period. Together, these are typical results for a CV, but the 626 s period is too long for a neutron star in a low-mass X-ray binary. The assumed WD nature of the compact object could be further tested with campaign of coherent timing of its rotation; long-term constancy would be expected for a WD, but not for a neutron star.

Our study identified two new CVs, Swift J0746.2–1611 and Swift J2218.4+1925. The latter is clearly an AM star with an orbital period of 129 min, while Swift J0746.2–1611 is of an uncertain type in which the secondary star is prominent in the spectrum and displays the 9.384 hr orbit. We estimated the secondary star as $K4\pm 2$ at a distance of 900(+190,–150) pc. At $V \sim 14.5$, Swift J0746.2–1611 is an easy target for additional searches for a spin period.

IGR J19552+0044 has a short but ambiguous orbital period, probably around 84 min. Its high-amplitude flickering with no coherent period, and large radial velocity amplitude, suggest that it may be an AM Her star. Follow-up studies, especially polarimetry, could better determine its nature.

We gratefully acknowledge support from NSF grants AST–0708810 and AST–1008217. We also thank Hwei-Ru Ong and Arlin Crofts for obtaining some of the optical spectra of IGR J19552+0044. The *XMM-Newton* observations of AX J1740.2–2903 and AX J1853.3–0128 were conducted by Eric Gotthelf, who first found their periodic signals. *XMM-Newton* is an ESA science mission with instruments and contributions directly funded by ESA Member States and NASA.

REFERENCES

- Ajello, M., Greiner, J., Rau, A., et al. 2006, ATel, 697
- Araujo-Betancor, S., Gänsicke, B. T., Hagen, H.-J., et al. 2005, A&A, 430, 629
- Baraffe, I., & Kolb, U. 2000, MNRAS, 318, 354
- Baumgartner, W. H., Tueller, J., Markwardt, C. B., Skinner, G. K., Barthelmy, S., Mushotzky, R. F., Evans, P., & Gehrels, N. 2012, ApJS, submitted, arXiv:1212.3336
- Bernardini, F., de Martino, D., Falanga, M., et al. 2012, A&A, 542, A22
- Bessell, M. S. 1990, PASP, 102, 1181
- Beuermann, K., Baraffe, I., & Hauschildt, P. 1999, A&A, 348, 524
- Beuermann, K., Harrison, T. E., McArthur, B. E., Benedict, G. F., & Gänsicke, B. T. 2003, A&A, 412, 821
- Beuermann, K., Harrison, T. E., McArthur, B. E., Benedict, G. F., & Gänsicke, B. T. 2004, A&A, 419, 291
- Bird, A. J., Bazzano, A., Bassani, L. et al. 2010, ApJS, 186, 1
- Bruch, A., & Engel, A. 1994, A&AS, 104, 79
- Butters, O. W., Barlow, E. J., Norton, A. J., & Mukai, K. 2007, A&A, 475, L29
- Capitano, F. Bird, A. J., Fiocchi, M., Scaringi, S., & Ubertini, P. 2011, ApJS, 195, 9
- Cusumano, G., La Parola, V., Segreto, A. et al. 2010a, A&A, 510, A48
- Cusumano, G., La Parola, V., Segreto, A. et al. 2010b, A&A, 524, A64
- Evans, P. A., Beardmore, A. P., & Osborne, J. P. 2008, ATel, 1669, 1
- Farrell, S. A., Gosling, A. J., Webb, N. A., et al. 2010, A&A, 523, A50
- Halpern, J. P., & Gotthelf, E. V. 2010, ATel, 2664
- Halpern, J. P., & Gotthelf, E. V. 2010, ATel, 2681
- Henden, A. A., Levine, S. E., Terrell, D., Smith, T. C., & Welch, D. 2012, Journal of the American Association of Variable Star Observers (JAAVSO), 40, 430
- Horne, K. 1986, PASP, 98, 609
- Hui, C. Y., Sriram, K., & Choi, C.-S. 2012, MNRAS, 419, 314

- Jenniskens, P., & Desert, F.-X. 1994, *A&AS*, 106, 39
- Kaplan, D. L., Gaensler, B. M., Kulkarni, S. R., & Slane, P. O. 2006, *ApJS*, 163, 344
- Keenan, P. C., & McNeil, R. C. 1989, *ApJS*, 71, 245
- Knigge, C. 2006, *MNRAS*, 373, 484
- Krivonos, R., Tsygankov, S., Revnivtsev, M., Grebenev, S. Churazov, E., & Sunyaev, R. 2010, *A&A*, 523, A61
- Kurtz, M. J. & Mink, D. J. 1998, *PASP*, 110, 934
- Landi, R., Masetti, N., Malizia, A., Bazzano, A., Flocchi, M., Bird, A. J., & Dean, A. J. 2008, *ATel*, 1437
- Landolt, A. U. 1992, *AJ*, 104, 340
- Malizia, A., Bassani, L., Sguera, V., et al. 2010, *MNRAS*, 408, 975
- Marsh, T., Littlefair, S., & Dhillon, V. 2006, *ATel*, 760
- Masetti, N., Bassani, L., Dean, A. J., Ubertini, P., & Walter, R. 2006, *ATel*, 735
- Masetti, N., Parisi, P., Palazzi, E., et al. 2009, *A&A*, 495, 121
- Masetti, N., Parisi, P., Palazzi, E., et al. 2010, *A&A*, 519, A96
- Masetti, N., Parisi, P., Jiménez-Bailón, E., et al. 2012, *A&A*, 538, A123
- Monet, D. G., Levine, S. E., Canzian, B., et al. 2003, *AJ*, 125, 984
- Muno, M. P., Gaensler, B. M., Nechita, A., Miller, J. M., & Slane, P. O. 2008, *ApJ*, 680, 639
- Nichelli, E., Israel, G. L., Moretti, A., et al. 2009, *ATel*, 2354
- Parisi, P., Masetti, N., Jimenez, E., Chavushyan, V., Bassani, L., Bazzano, A., & Bird, A. J. 2008, *ATel*, 1710
- Patterson, J., Thorstensen, J. R., Vanmunster, T., et al. 2004, *PASP*, 116, 516
- Patterson, J., Halpern, J., Mirabal, N., Christe, G., McCormick, J., Rea, R., & Messier, D. 2006, *ATel*, 757
- Peters, C. S., & Thorstensen, J. R. 2005, *PASP*, 117, 1386
- Ritter, H., & Kolb, U. 2003, *A&A*, 404, 301
- Rodríguez-Gil, P., Gänsicke, B. T., Araujo-Betancor, S., & Casares, J. 2004, *MNRAS*, 349, 367

- Roeser, S., Demleitner, M., & Schilbach, E. 2010, *AJ*, 139, 2440
- Sakano, M., Torii, K., Koyama, K., Maeda, Y., & Yamauchi, S. 2000, *PASJ*, 52, 1141
- Scaringi, A., Bird, A. J., Norton, A. J., et al. 2010, *MNRAS*, 401, 2307
- Schlafly, E. F. & Finkbeiner, D. P. 2011, *ApJ*, 737, 103
- Schlegel, D. J., Finkbeiner, D. P., & Davis, M. 1998, *ApJ*, 500, 525
- Schneider, D., & Young, P. 1980, *ApJ*, 238, 946
- Schwobe, A. D., Schwarz, R., Staude, A., et al. 1999, *Annapolis Workshop on Magnetic Cataclysmic Variables* (ed. C. Hellier & K. Mukai), ASPC, 157, 71
- Shafter, A. W. 1983, *ApJ*, 267, 222
- Steeghs, D., Knigge, C., Drew, J., Unruh, Y., & Greimel, R. 2008, *ATel*, 1653
- Thorstensen, J. R., & Freed, I. W. 1985, *AJ*, 90, 2082
- Thorstensen, J. R., Patterson, J., Thomas, G., & Shambrook, A. 1996, *PASP*, 108, 73
- Thorstensen, J. R., Patterson, J., Halpern, J., & Mirabal, N. 2006, *ATel*, 767
- Thorstensen, J. R., & Halpern, J. P. 2009, *ATel*, 2177
- Thorstensen, J. R., & Skinner, J. N. 2012, *AJ*, 144, 81
- Tomsick, J. A., Rodriguez, J., Chaty, S., Walter, R., & Kaaret, P. 2008, *ATel*, 1649
- Tomsick, J. A., Chaty, S., Rodriguez, J., Walter, R., & Kaaret, P. 2009, *ApJ*, 701, 811
- Tonry, J. & Davis, M. 1979, *AJ*, 84, 1511
- Torres, M. A. P., Steeghs, D., Garcia, M. R., et al. 2006, *ATel*, 763
- Voss, R., & Ajello, M. 2010, *ApJ*, 721, 1843
- Warner, B., in *Cataclysmic Variable Stars*, 1995, Cambridge University Press, New York
- Wheatley, P. J., Marsh, T. R., & Clarkson, W. 2006, *ATel*, 765
- Witham, A. R., Knigge, C., Aungwerojwit, A., et al. 2007, *MNRAS*, 382, 1158
- Zacharias, N., Finch, C., Girard, T., et al. 2010, *AJ*, 139, 2184
- Zacharias, N., Finch, C. T., Girard, T. M., et al. 2013, *AJ*, 145, 44
- Yuan, H. B., & Liu, X. W. 2012, *MNRAS*, 425, 1763

Table 1. Stars Observed

Name	R.A. (h m s)	Decl. (° ' ")	V	Ref ^a	Data ^b	Class ^c	P (s)	Ref ^d
1RXS J045707.4+452751	04 57 08.32	+45 27 50.0	17.5	S	S,T	DQ	1218.7(5)	1
Swift J0732.5–1331 ^e	07 32 37.71	–13 31 08.3	15.7	D	S	DQ	512.42(3)	2
Swift J0746.2–1611	07 46 17.11	–16 11 27.7	14.5	A	S,X	N		
AX J1740.2–2903	17 40 16.10	–29 03 38.1	19.1	S	S,X,T	DQ	628.6(2.3)	1
IGR J18173–2509	18 17 22.18	–25 08 42.6	16.9	D	S	DQ	1663.4(1.4)	3
IGR J18308–1232	18 30 49.94	–12 32 19.1	17.9	D	S	DQ	1820(2)	3
AX J1853.3–0128	18 53 30.60	–01 28 15.9	16:	B	S,X,T	DQ	477.6(1.0)	1
IGR J19267+1325	19 26 27.00	+13 22 04.9	18:	I	S,T	DQ	935.1(2)	1
IGR J19552+0044	19 55 12.47	+00 45 36.6	16: ^f	B	S,T	AM?		
Swift J2218.4+1925	22 18 32.76	+19 25 20.5	17.5	B	S,X	AM		

Note. — Coordinates are for J2000.0 (ICRS), either from the PPMXL catalogue (Roeser et al. 2010) or derived from astrometric fits to our own images referred to the UCAC-3 (Zacharias et al. 2010). Estimated uncertainty is $\pm 0''.2$.

^aSource of approximate V magnitude: S = our spectrophotometry; D = our direct image; A = APASS (Henden et al. 2012), as listed in the UCAC-4 (Zacharias et al. 2013); B = interpolated from Schmidt-plate magnitudes in USNO-B1.0; I = extrapolated from IPHAS, $r' = 17.7$ (Steehgs et al. 2008). (Monet et al. 2003), as listed in PPMXL (Roeser et al. 2010).

^bTypes of data presented here; S = time-resolved spectroscopy; T = time series photometry; X = X-ray light curve.

^cClassifications are: N = novalike variable (pulsations not confirmed); DQ = DQ Her star or IP (evidence for pulsations); AM = AM Her star or polar.

^dReference for period P , presumed to be the spin period: (1) this paper, optical; (2) Patterson et al. 2006, optical; (3) Bernardini et al. 2012, X-ray.

^eNow named V667 Puppis

^fCatalogued magnitudes of this object show variability by ~ 2 mag.

Table 2. Radial Velocities

Star ^a	Time ^b	v_{abs} (km s ⁻¹)	σ (km s ⁻¹)	v_{emn} (km s ⁻¹)	σ (km s ⁻¹)
RX J0457	55128.9305	-3	7
RX J0457	55128.9373	4	5
RX J0457	55128.9578	-8	5
RX J0457	55128.9654	-19	6
RX J0457	55129.7049	39	8
RX J0457	55129.7153	35	6
RX J0457	55129.7254	20	5

^aAbbreviated star name.

^bHeliocentric Julian Date of mid-exposure minus 2400000; the time base is UTC.

Note. — Table 2 is published in its entirety in the electronic edition of The Astronomical Journal, A portion is shown here for guidance regarding its form and content.

Table 3. Fits to Radial Velocities

Data set	T_0^a	P_{spec} (d)	K (km s ⁻¹)	γ (km s ⁻¹)	N	σ^b (km s ⁻¹)
1RXS J045707.4+452751	55221.924(6)	0.257819 ^c	44(6)	-25(5)	60	21
(alternate)	55221.875(5)	0.200424 ^c	46(6)	-27(5)	60	21
Swift J0732.5-1331	53812.7591(14)	0.2338(2)	149(5)	20(4)	50	18
Swift J0746.2-1611 (absn)	55279.663(3)	0.391012(11)	90(4)	53(3)	47	13
(emission)	55279.524(9)	0.39097(3)	54(6)	35(5)	48	21
(combined)	...	0.391006(10)	
AX J1740.2-2903	55736.8052(19)	0.2384(5)	110(6)	42(4)	29	18
IGR J18173-2509	55365.6931(17)	0.06382(8)	47(8)	44(6)	35	22
IGR J18308-1232	55734.698(2)	0.2239(5)	104(9)	-6(5)	49	26
AX J1853.3-0128	56078.7312(9)	0.06058(7)	42(4)	-53(3)	30	12
IGR J19267+1325 (2008 Sep)	54712.6507(17)	0.1455(8)	80(6)	16(4)	45	16
(2009 Jun)	54996.885(3)	0.1432(4)	72(6)	25(5)	13	14
(combined)	54712.6504(20)	0.1437(4)	79(7)	17(5)	45	19
IGR J19552+0044	56274.6121(20)	0.058051 : ^d	170(33)	-9(24)	97	112
Swift J2218.4+1925	55070.6819(9)	0.08996(9)	344(26)	25(16)	32	71

Note. — Parameters of least-squares fits to the radial velocities, of the form $v(t) = \gamma + K \sin [2\pi(t - T_0)/P_{\text{spec}}]$.

^aHeliocentric Julian Date minus 2400000. The epoch is chosen to be near the center of the time interval covered by the data, and within one cycle of an actual observation.

^bRoot-mean-square residual of the fit.

^cThe two periods reflect different choices of daily cycle count, and the excessively precise periods tabulated here reflect in turn an arbitrary choice of cycle count between observing runs. For each choice of daily cycle count, we estimate the uncertainty in the gross period to be 0.008 d.

^dThis period was used in the fit, but it is highly uncertain – see Section 3.9 and Figure 14.

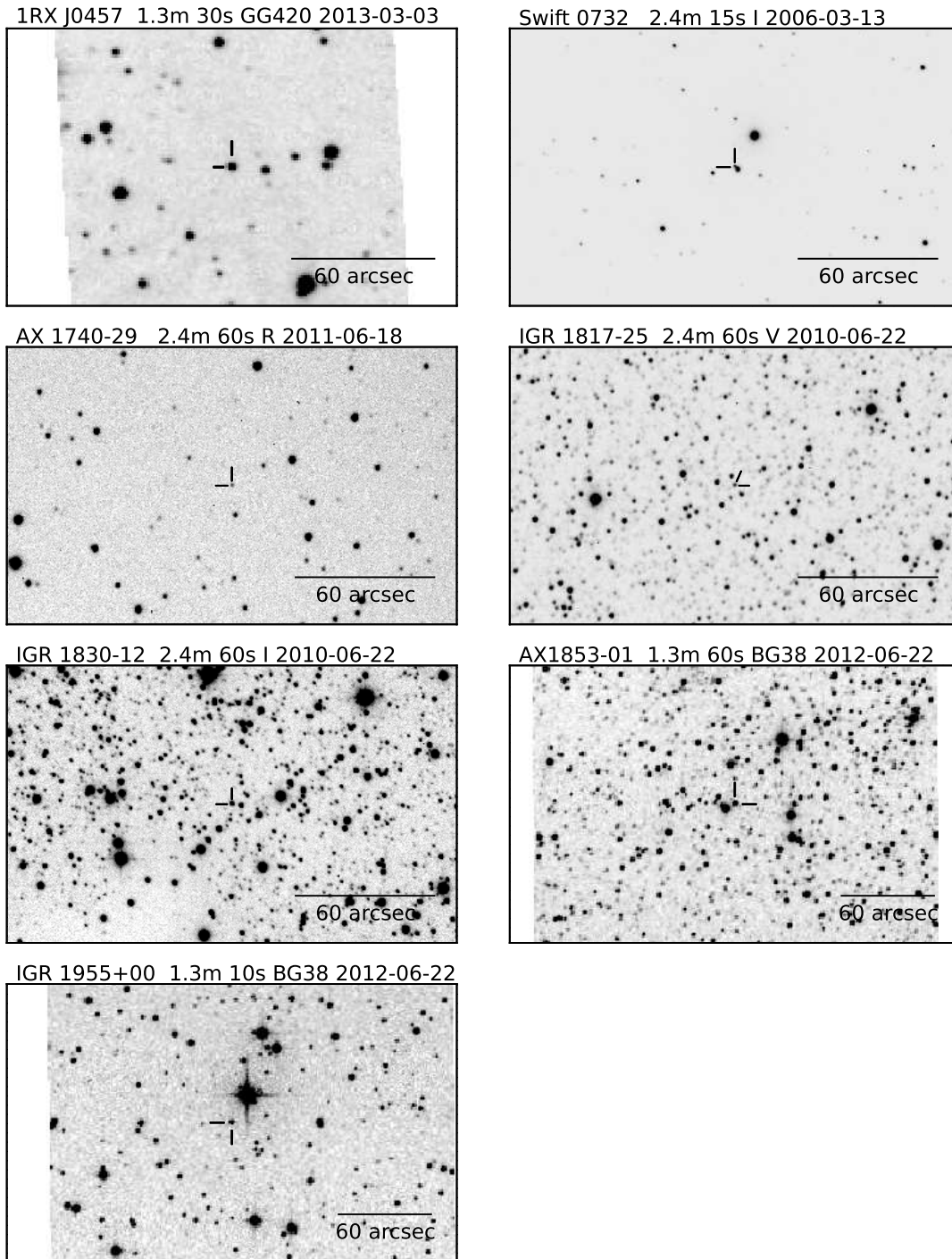


Fig. 1.— Finding charts for some of the objects. North is up, east is to the left, and the scale is indicated. The label on each Figure gives the source of the image used, and the tick marks are accurately aligned with the coordinates in Table 1. Shortened names are used; “Swift 0732” is V667 Puppis. The chart for 1RXS J045707.4+452751 supersedes the incorrect chart in Masetti et al. (2010).

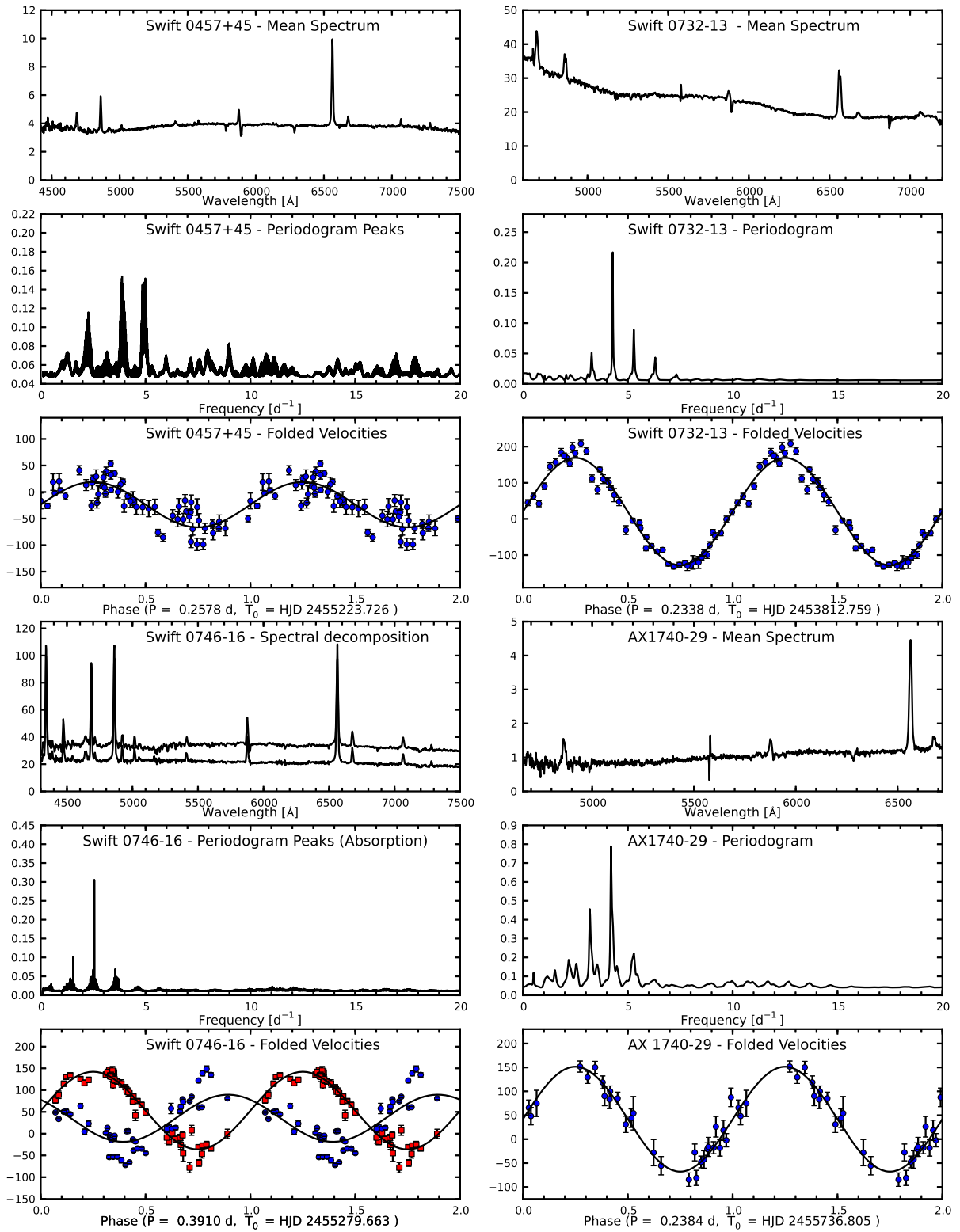


Fig. 2.— Mean spectra, periodograms, and folded velocity curves for four of the objects. The units of the vertical axes of the spectra are $10^{-16} \text{ erg cm}^{-2} \text{ s}^{-1} \text{ \AA}^{-1}$; for the periodograms, the axis is unitless ($1/\chi^2$); and the radial velocities are in km s^{-1} . In the velocity curves, all data are repeated on an extra cycle for continuity, the uncertainties shown are estimated from counting statistics, and the solid curves show the best-fitting sinusoids. In the spectrum of Swift J0746.2–1611, the lower trace shows the result of subtracting a K4V-type spectrum, scaled to $V = 16.36$. Circles (blue in on-line version) are emission-line velocities and squares (in the case of Swift J0746.2–1611; red in on-line version) are absorption-line velocities of the secondary star.

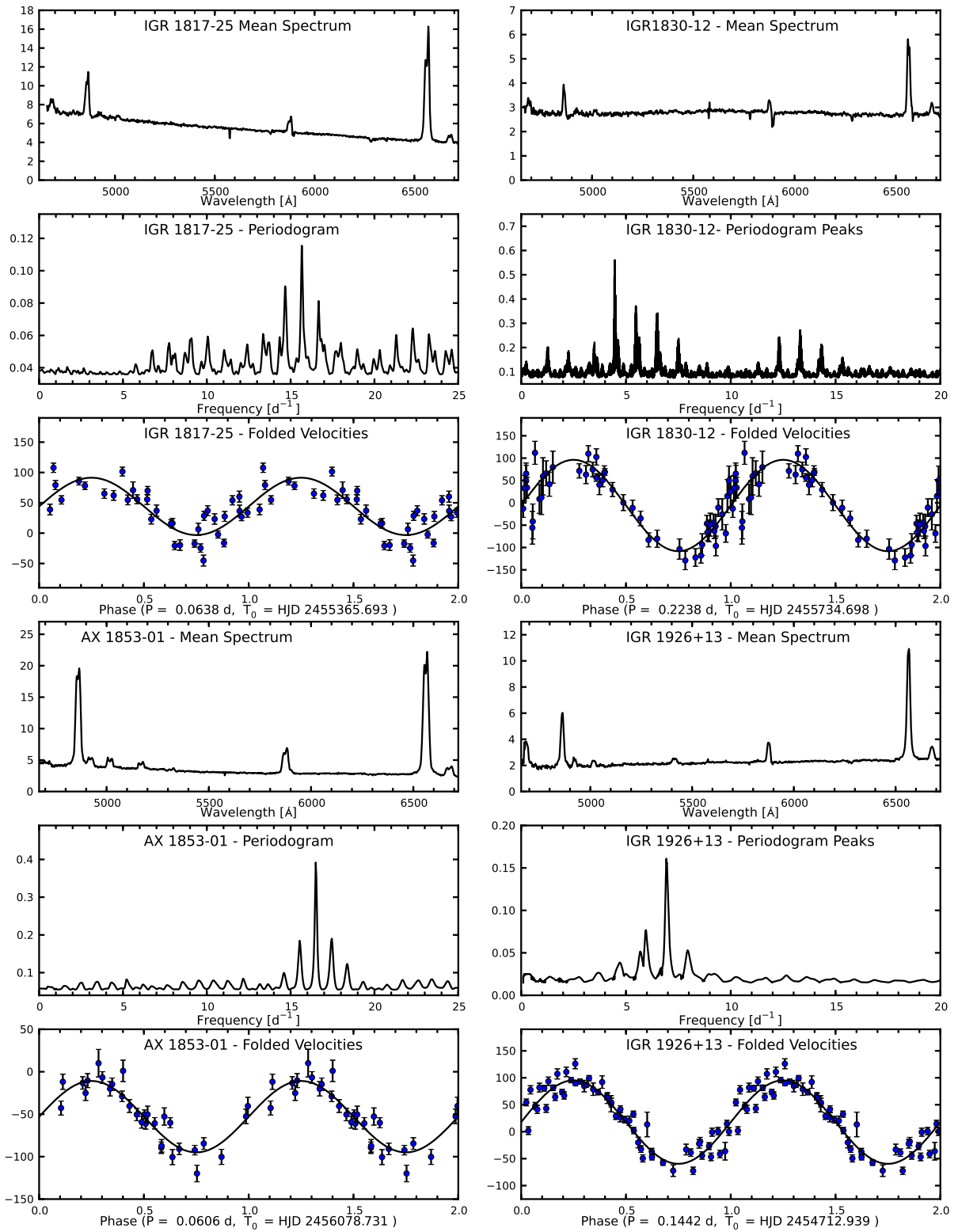


Fig. 3.— Same as Figure 2, for four other objects.

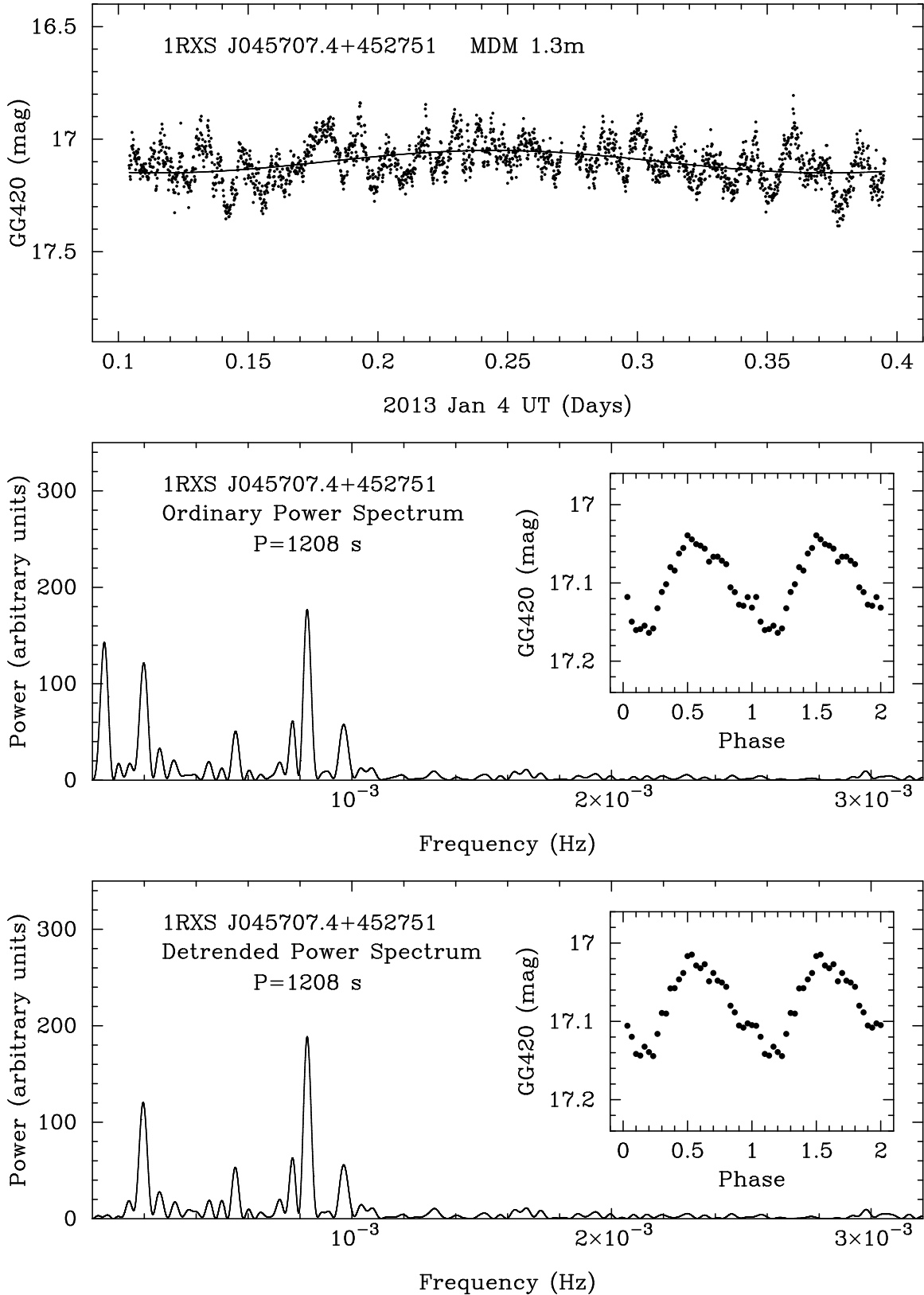


Fig. 4.— Time-series photometry of 1RXS J045707.4+452751, with power spectra before and after “detrending” the data with a 0.258-d period. Individual exposures are 12 s. The rough calibration uses the R magnitude of the comparison star from the USNO-B1.0 catalog. The insets show the mean pulse profile folded at 1208 s.

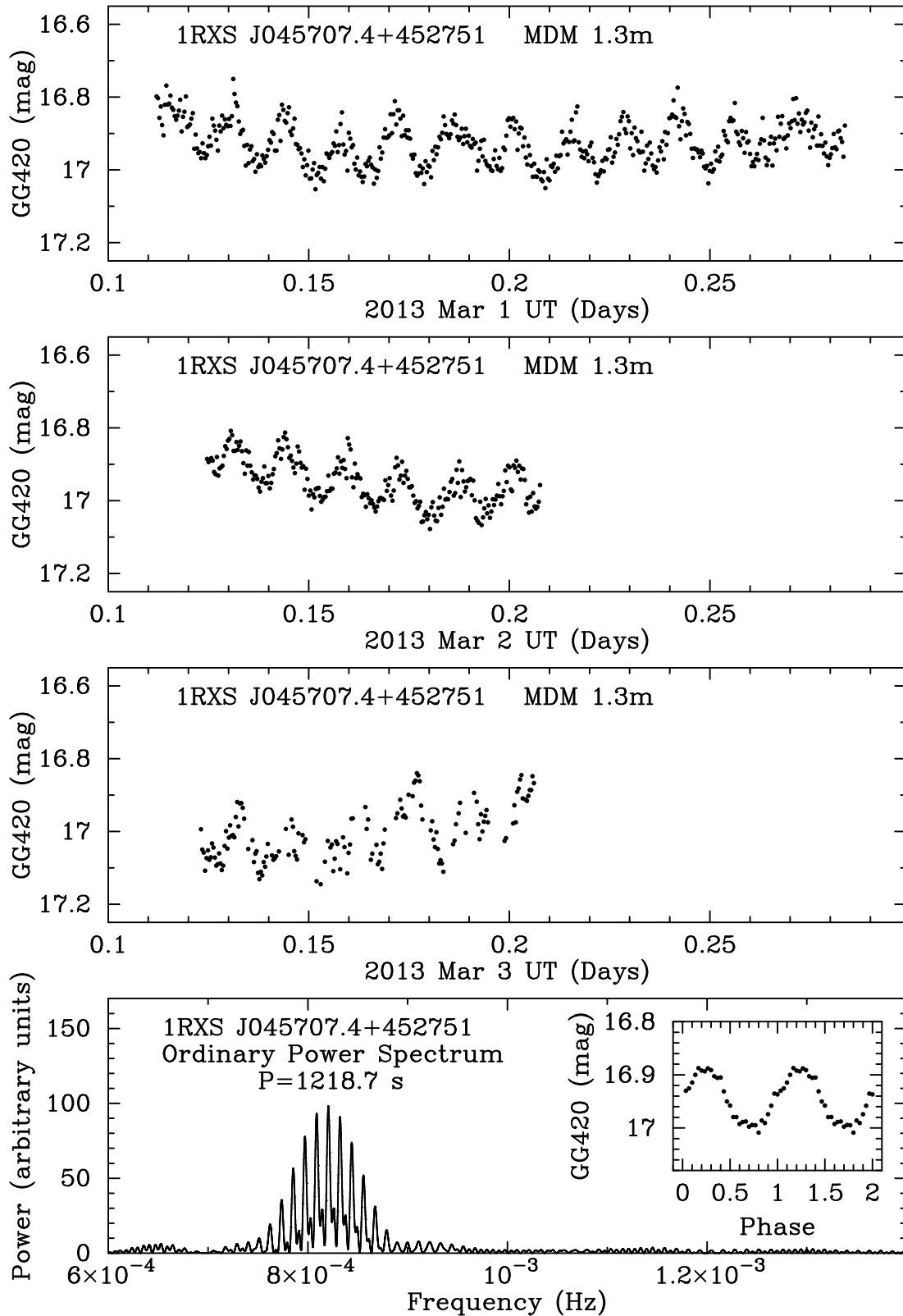


Fig. 5.— More time-series photometry of 1RXS J045707.4+452751. Individual exposures are 30 s. A coherent power spectrum of the three consecutive nights gives a best fitted period of 1218.7 ± 0.5 s.

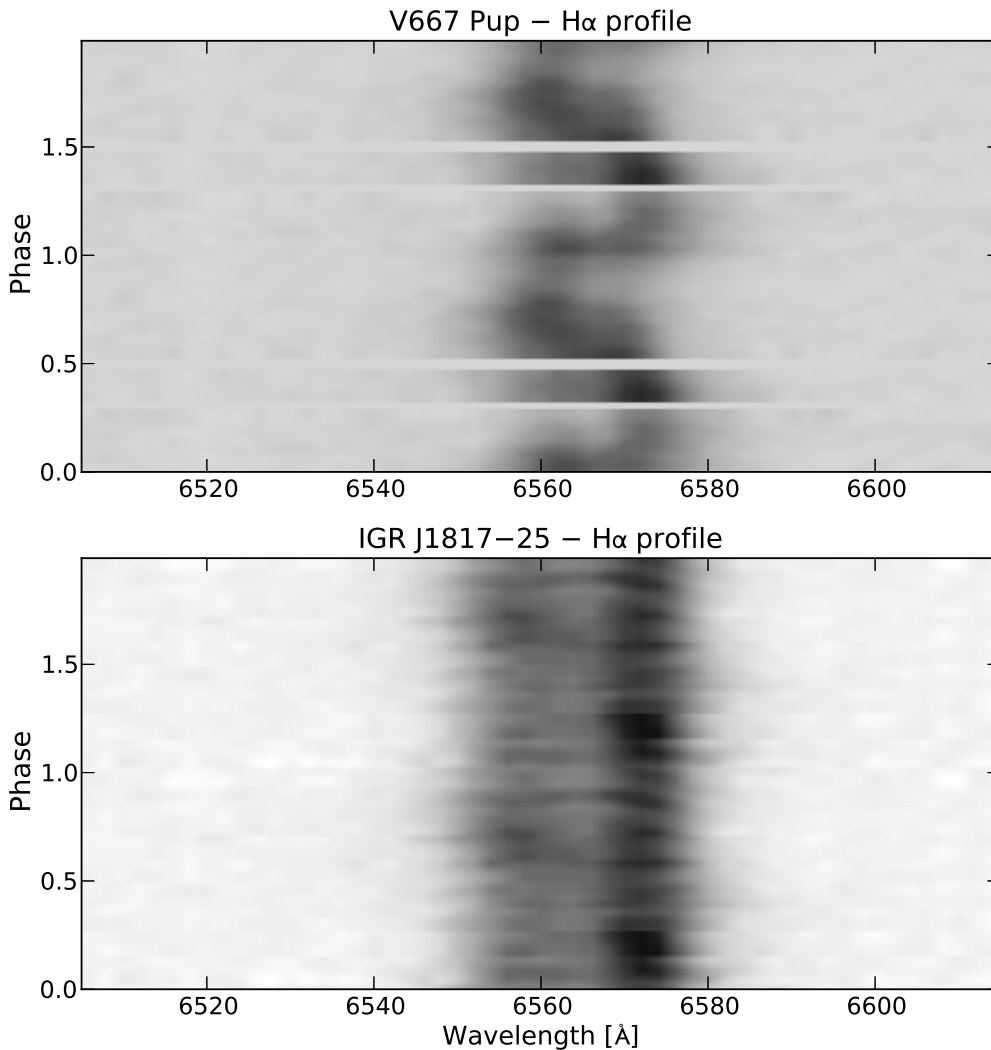


Fig. 6.— Upper: Greyscale representation of the H α profile of V667 Puppis (Swift J0732.5–1331) as a function of orbital phase (using the ephemeris of Table 3). The data are repeated for a second cycle, and the blank horizontal bars are gaps in coverage. Lower: A similar display of the H α profile for IGR J18173–2509. Each line in the image represents an average of spectra near that phase, as described in Section 3.2.

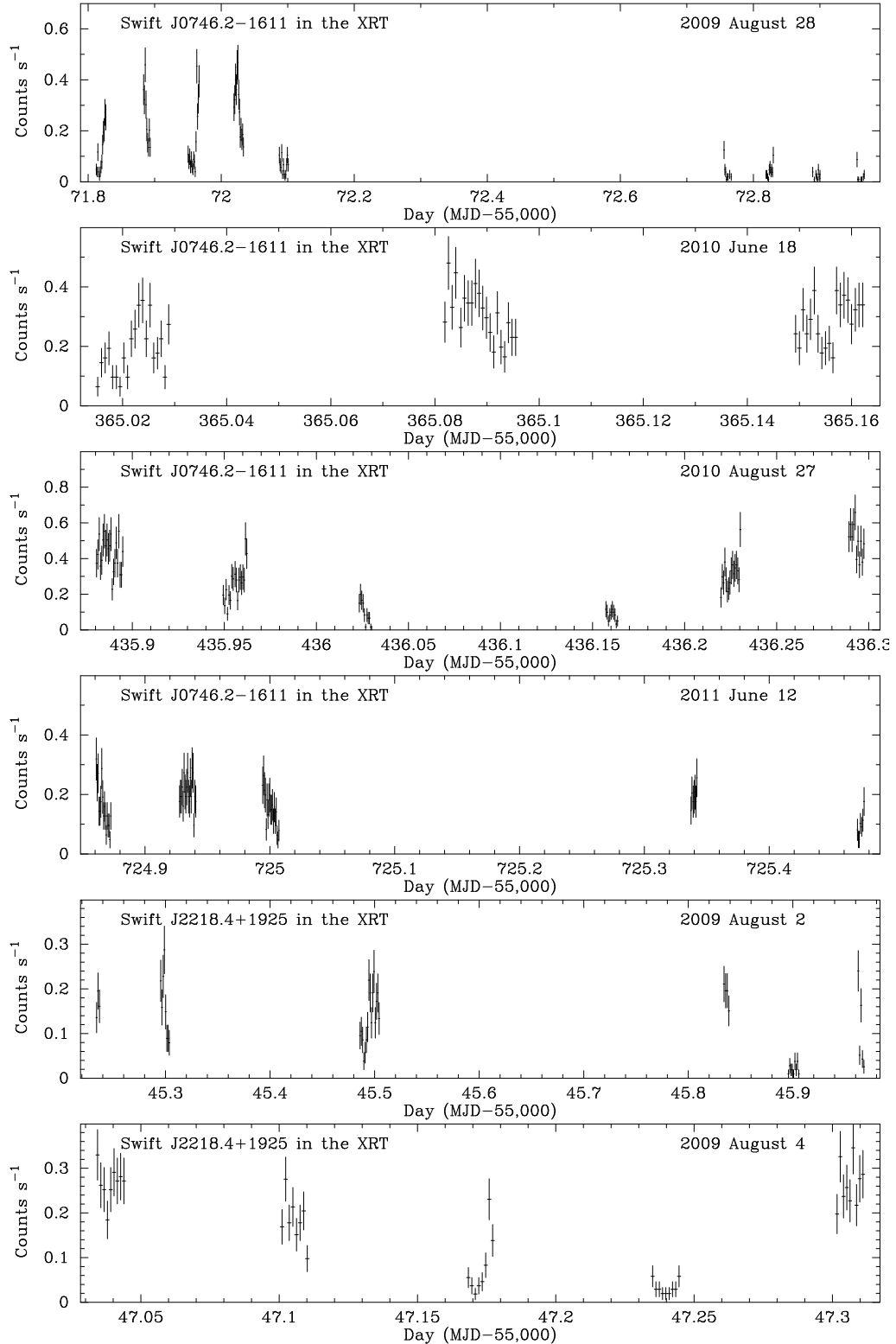


Fig. 7.— Light curves of Swift J0746.2–1611 and Swift J2218.4+1925 in the 0.3–10 keV band from the *Swift* XRT.

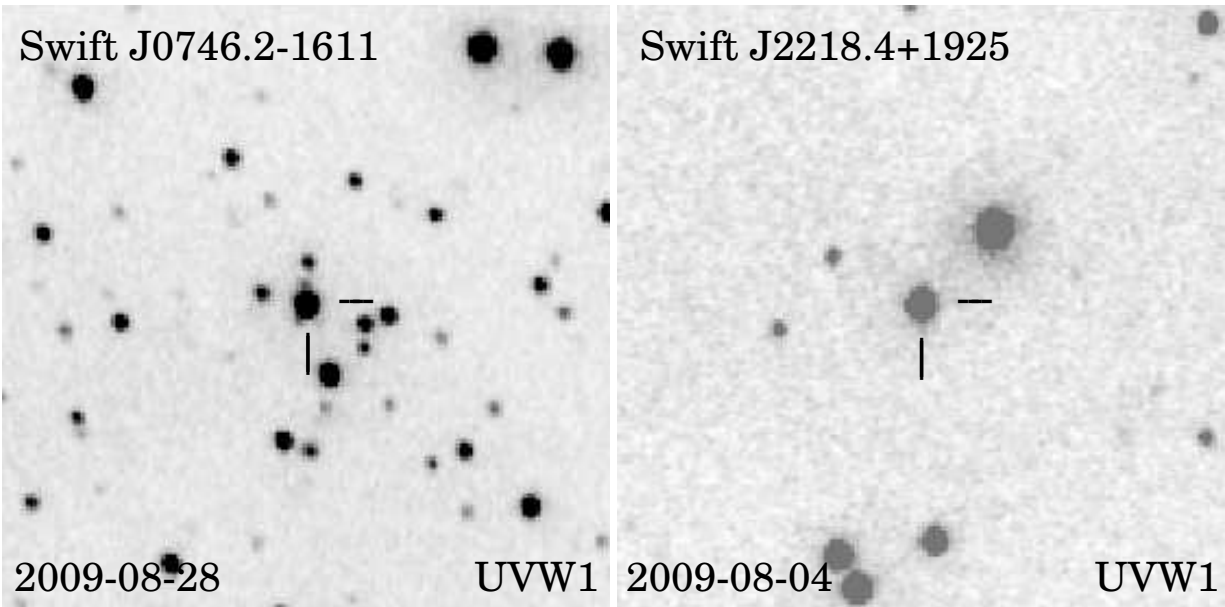


Fig. 8.— Finding charts for Swift J0746.2–1611 and Swift J2218.4+1925 in the *Swift* UVOT. Coordinates are given in Table 1. Each image cutout is $3' \times 3'$. North is up and east is to the left.

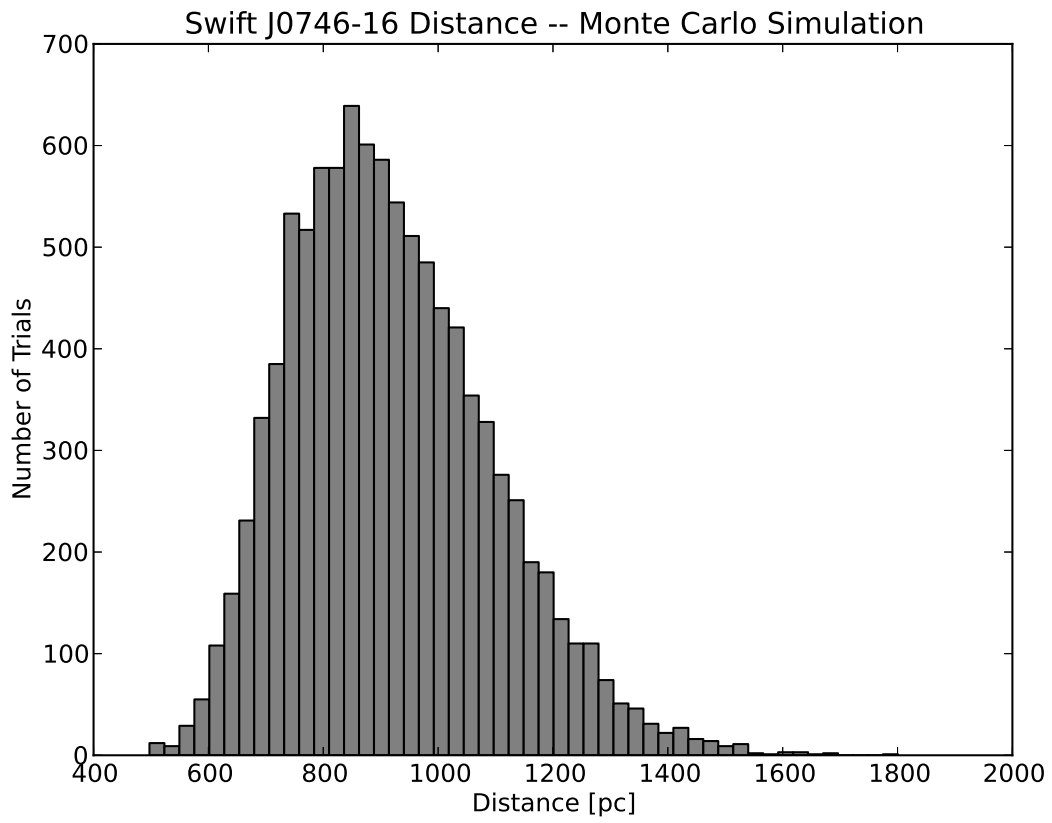


Fig. 9.— Distribution of distance estimates for Swift J0746.2–1611, from 10,000 calculations using randomized input parameters.

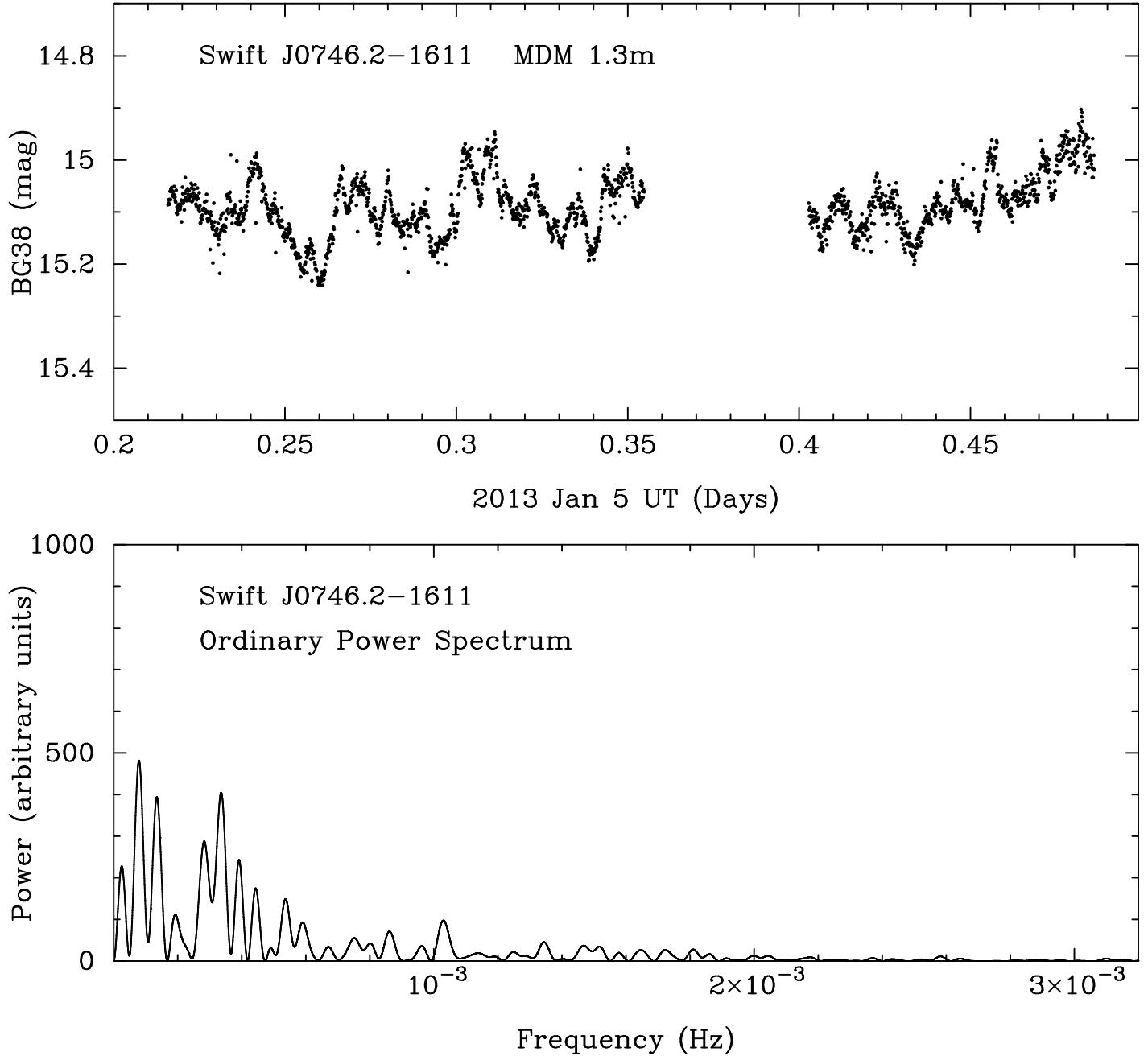


Fig. 10.— Time-series photometry of Swift J0746.2–1611. Individual exposures are 10 s. Power spectrum analysis of this and other light curves of this star do not reveal a period.

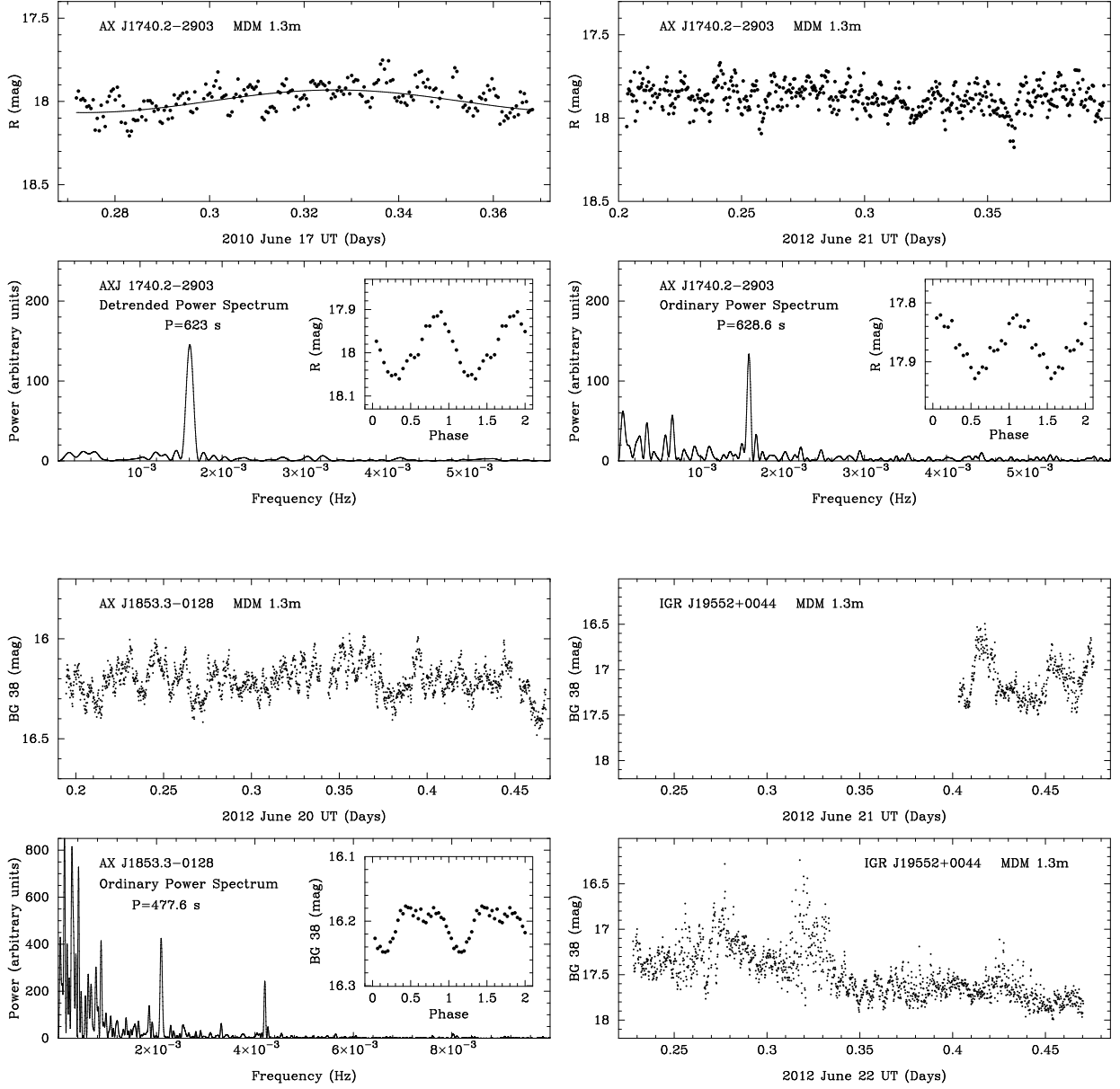


Fig. 11.— Time-series photometry obtained on the 1.3m McGraw-Hill telescope. Individual exposures are 30 s in R for AX J1740.2–2903, and 10 s in BG38 for AX J1853.3–0128 and IGR J19552+0044. In cases where spin periods are detected, the power spectrum, period, and binned pulse profile (insets) are given in the panel below the light curve. In one case a broad trend (solid curve) was subtracted from the data before calculating the “detrended” power spectrum. Magnitude calibration in R is from Landolt standard stars. In the BG38 filter, a rough calibration averaging B and R magnitudes from the USNO-B1.0 catalog is used.

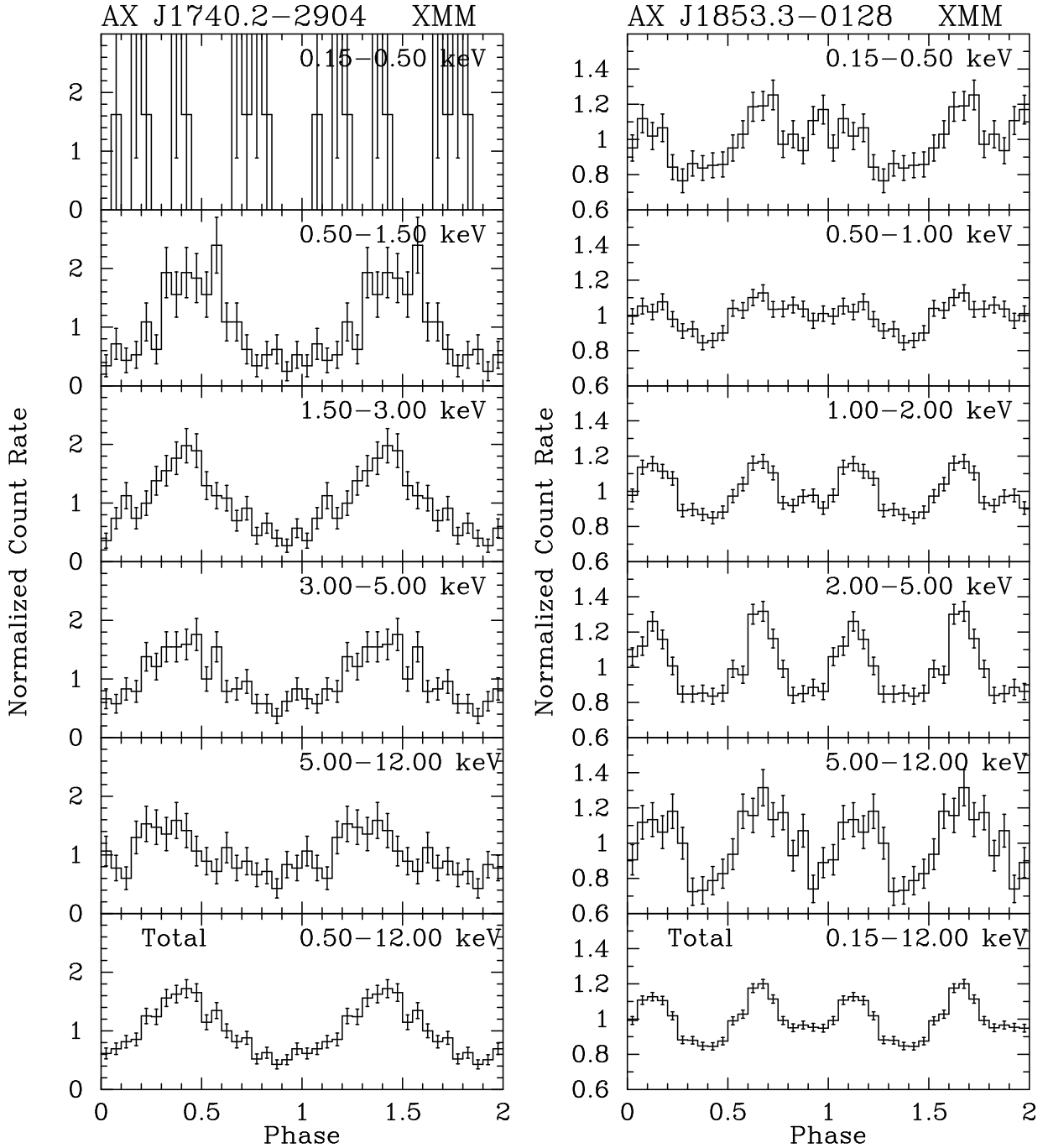


Fig. 12.— Energy-dependent X-ray pulse profiles from *XMM-Newton* observations. Left: AX J1740.2–2903 folded on its period of 623 s, from an observation on 2005 September 29 (ObsID 03042201). Right: AX J1853.3–0128 folded on its true 476 s period, from an observation on 2004 October 25 (ObsID 02015003). The pulse shape as a function of energy changes from primarily a single, broad plateau at energies < 1 keV (resembling the optical pulse), to double peaked at high energies.

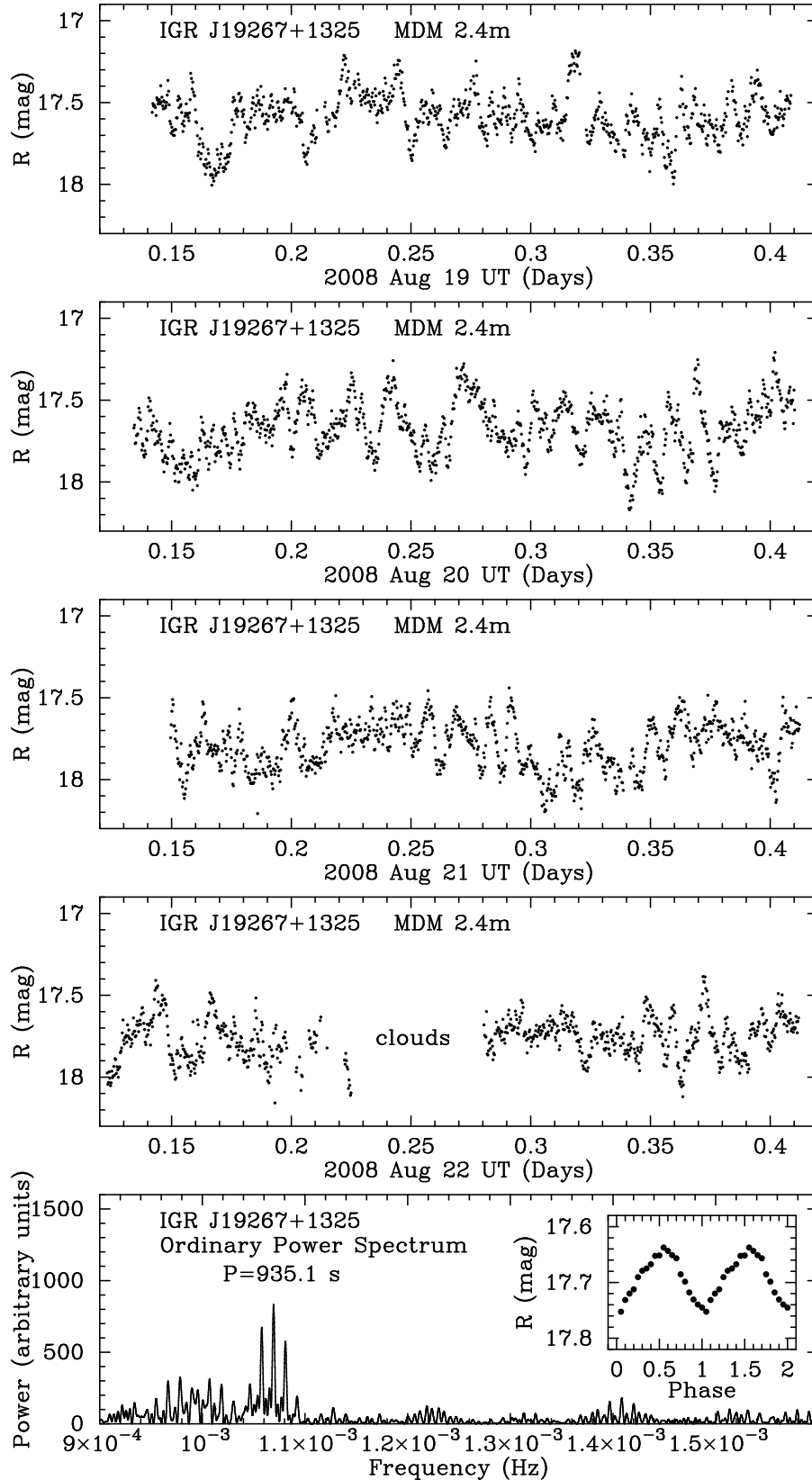


Fig. 13.— Time-series CCD photometry of IGR J19267+1325 on four consecutive nights. Individual exposures are 10 s in R . The coherent power spectrum of the four nights and the folded light curve are given in the bottom panel. The measured spin period is 935.1 ± 0.2 s.

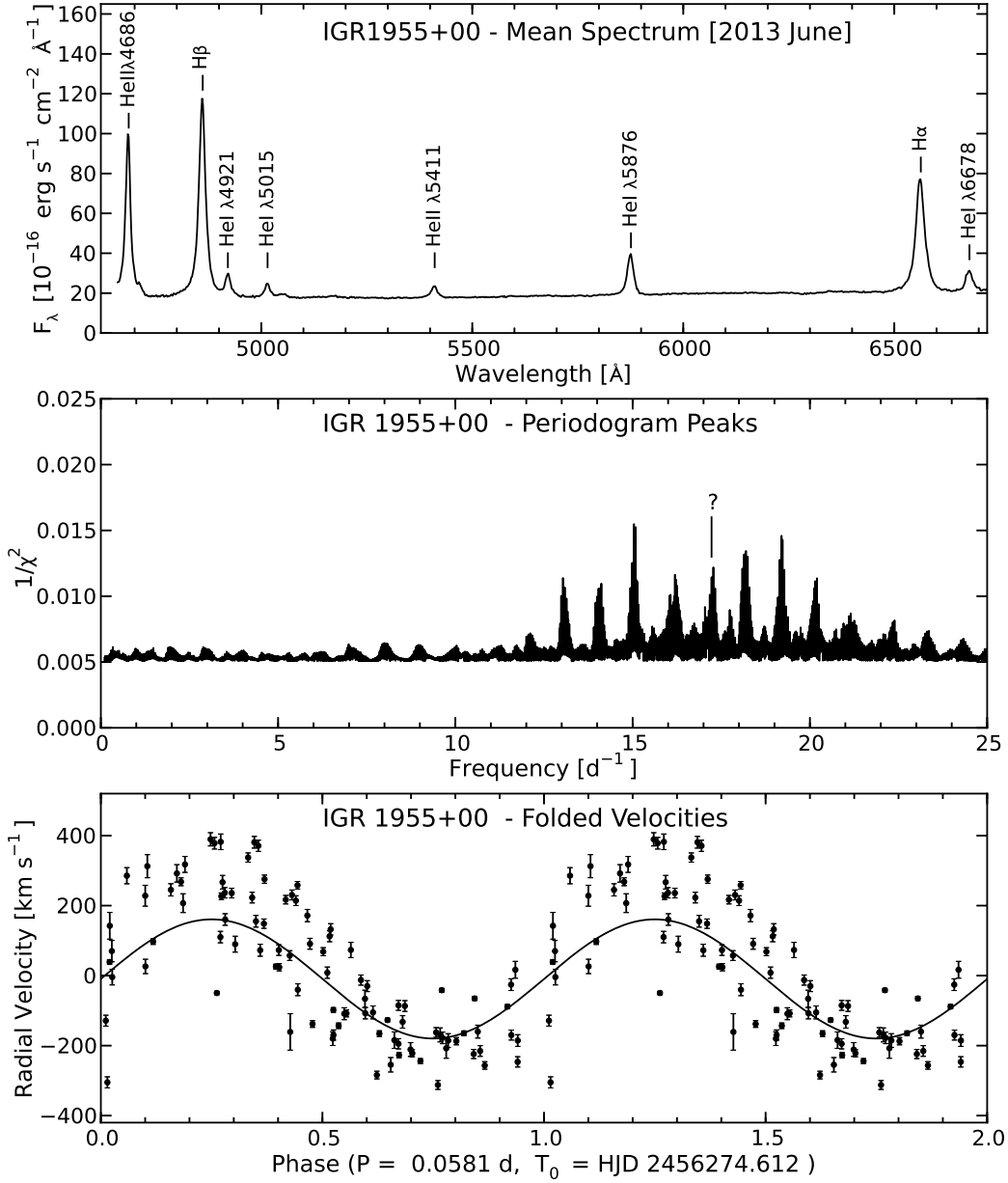


Fig. 14.— Top panel: Mean spectrum of IGR J19552+0044 from 2013 June. Middle panel: Period search of H α radial velocities of IGR J19552+0044. The full periodogram is not shown; rather, the curve connects local maxima. Lower panel: H α radial velocities folded on the adopted period, which is uncertain. A sinusoid fitted at this period (Table 3) is also shown.

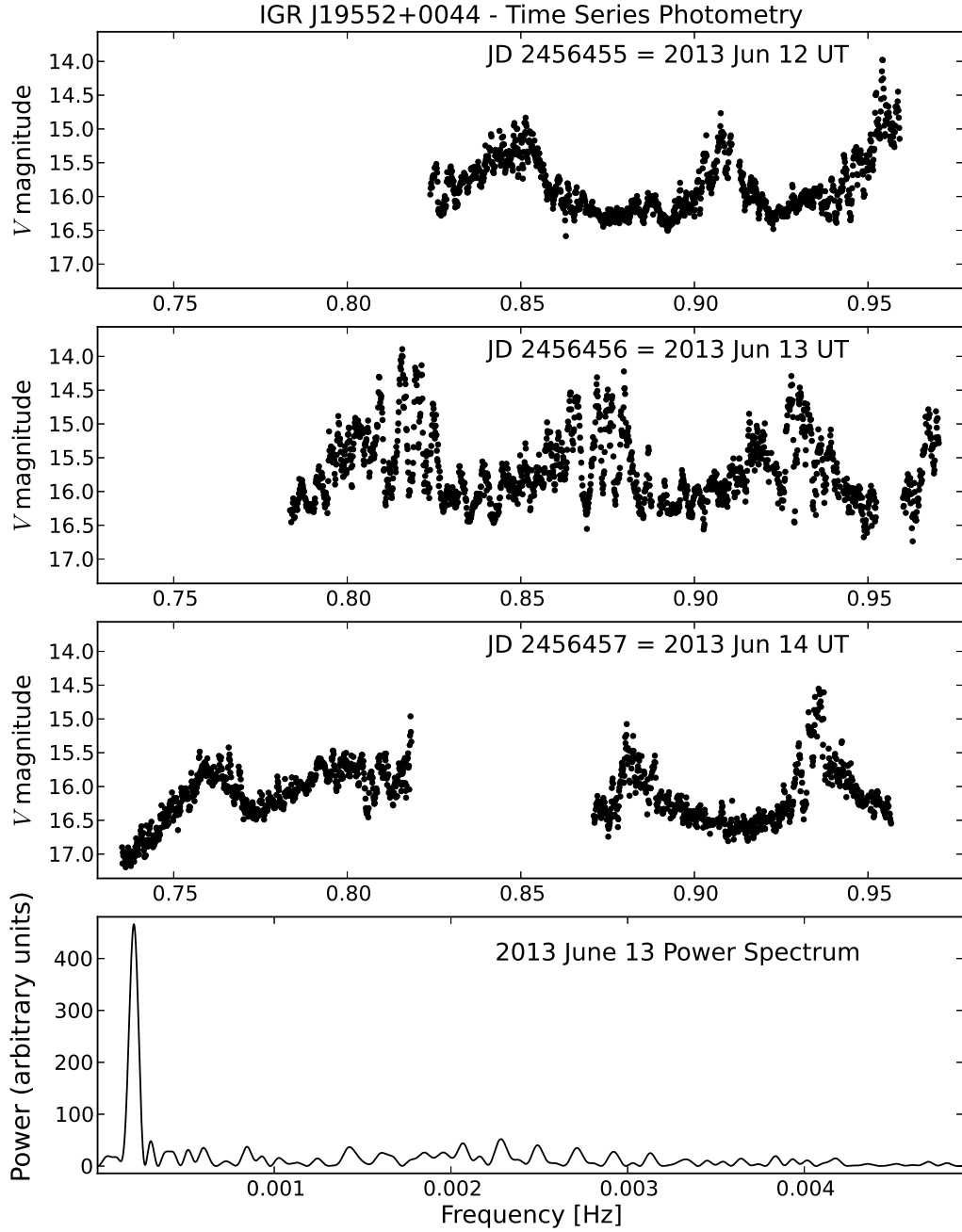


Fig. 15.— Time-series photometry of IGR J19552+0044 obtained in 2013 June. For the top three panels, the horizontal axes show fractional days on the dates indicated. The lower panel shows a power spectrum for June 13; the peak at low frequency corresponds to the ~ 81 min modulation evident in the light curve. The absence of other peaks indicates that the large-amplitude flickering on that night does not arise from a coherent periodicity.

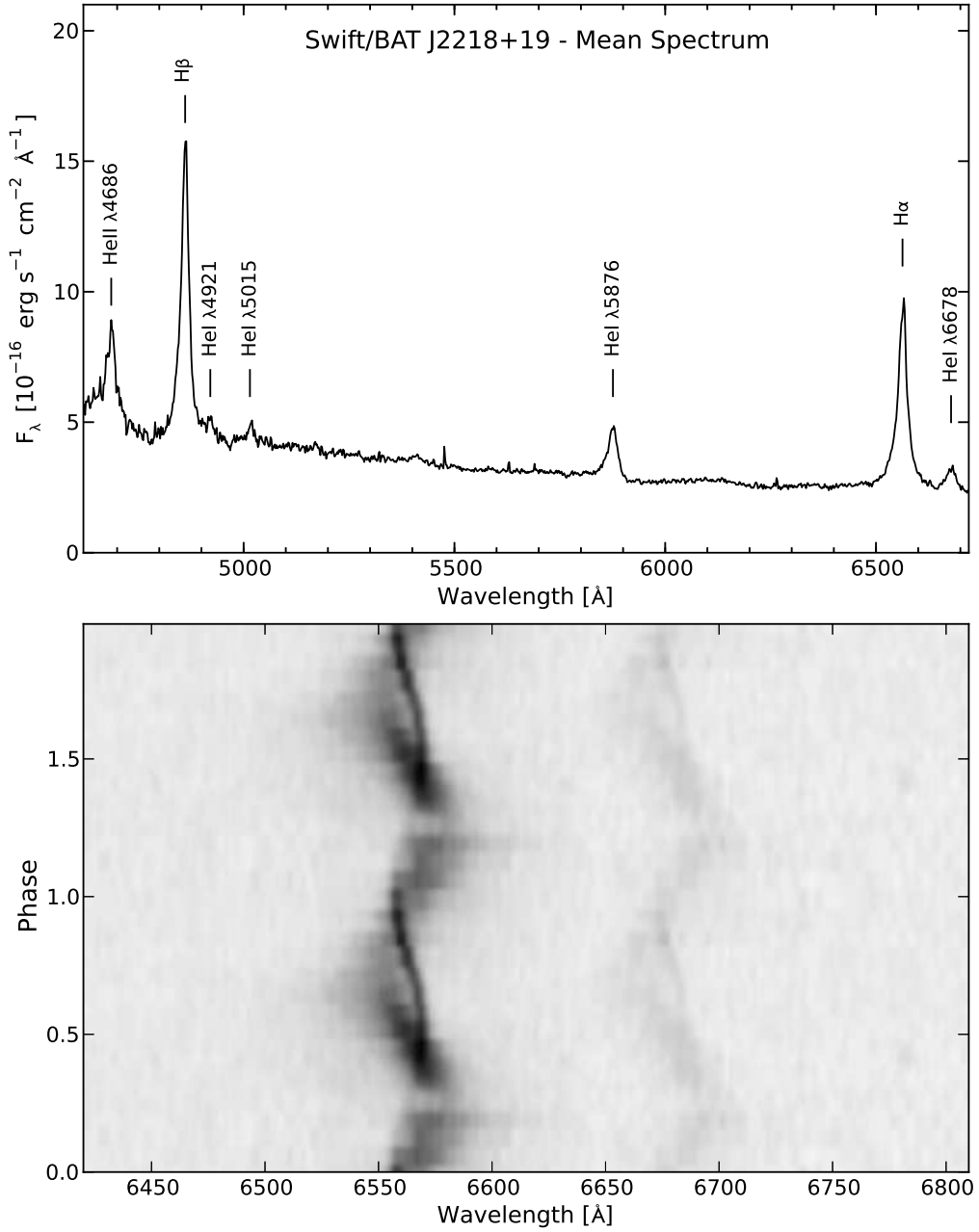


Fig. 16.— Upper panel: Mean spectrum of Swift J2218.4+1925. The more prominent emission lines are identified. Lower panel: A greyscale representation of the region of the H α and He I λ 6678 emission lines, plotted as a function of orbital phase. Phase increases from the bottom, and two cycles are shown for continuity. The spectrum is represented as a negative (i.e., larger fluxes are shown as darker pixels). The phase is computed from the values of T_0 and P_{spec} listed in Table 3. See Section 3.2 for procedural details.